Earth-Science Reviews 242 (2023) 104432

Contents lists available at ScienceDirect

Earth-Science Reviews

journal homepage: www.elsevier.com/locate/earscirev

The response and sensitivity of deuterium and ^{17}O excess parameters in precipitation to hydroclimate processes

Zhengyu Xia [a,b,*], Jakub Surma [c,d], Matthew J. Winnick [b]

[a] Key Laboratory of Geographical Processes and Ecological Security in Changbai Mountains, Ministry of Education, School of Geographical Sciences, Northeast Normal University, Changchun, China
[b] Department of Geosciences, University of Massachusetts Amherst, Amherst, MA, USA
[c] Department of Earth and Planetary Sciences, Tokyo Institute of Technology, Tokyo, Japan
[d] Geoscience Center, Georg-August University, Göttingen, Germany

ARTICLE INFO

Keywords:
Water isotopes
Deuterium excess
Triple oxygen isotopes
Water cycle
Fractionation

ABSTRACT

The new excess term of the triple oxygen isotope composition in meteoric water, expressed as $\Delta'^{17}O$, is conceived to track the component of kinetic fractionation in the water cycle, much like the traditional deuterium excess (d-excess) based on dual hydrogen and oxygen isotope compositions. Here, we use theoretical models to investigate the common and distinct features of variations in these two parameters that result from isotopic fractionation in each step of the water cycle. The objective is to demonstrate their different responses and sensitivities to hydroclimate processes and to explore an interpretive framework based on paired precipitation d-excess and $\Delta'^{17}O$ data.

For oceanic evaporation as the first step of the water cycle, both models and observations suggest that the d-excess and $\Delta'^{17}O$ of oceanic evaporation fluxes commonly respond to relative humidity as well as boundary-layer aerodynamics and isotopic gradients at the site of evaporation, reflecting similar moisture source information on short timescales. As the isotopic signal of oceanic vapor is transmitted to precipitation, d-excess and $\Delta'^{17}O$ show distinct non-conservative behaviors in condensation and Rayleigh distillation, which result in decoupling between d-excess and $\Delta'^{17}O$ in precipitation. This decoupling is particularly pronounced when the degree of distillation is small. Additionally, we develop a new model to show that the interaction between vapor mixing and distillation causes lower $\Delta'^{17}O$ in precipitation than in the case of Rayleigh distillation without the presence of external vapor sources, whereas only minimal effects are observed in d-excess. Furthermore, we find that precipitation $\Delta'^{17}O$ has a relatively higher sensitivity than d-excess to terrestrial evaporation-dominated moisture recycling and re-evaporation of raindrops in light rains. Finally, we develop stochastic model simulations to show that the idealized Rayleigh distillation model modified to incorporate the raindrop re-evaporation/equilibration and vapor mixing is sufficient to reproduce the observed patterns in the relationships among $\delta^{18}O$, d-excess, and $\Delta'^{17}O$ in precipitation.

This forward-looking review built on the analysis of theoretical models highlights new opportunities in leveraging the joint information from precipitation d-excess and $\Delta'^{17}O$ data to fingerprint water cycle processes at a range of spatiotemporal scales. However, we also emphasize the challenges associated with these complex and opaque tracers, which aggregate multiple fractionation steps within the water cycle. We suggest that site-specific, multiple-year 12 monthly means of paired precipitation d-excess and $\Delta'^{17}O$ data are most useful to disentangle their complex controls. This effort will provide a mechanistic basis for future applications of triple oxygen isotope techniques in geological records for paleo-reconstructions.

* Corresponding author at: Key Laboratory of Geographical Processes and Ecological Security in Changbai Mountains, Ministry of Education, School of Geographical Sciences, Northeast Normal University, Changchun, China.
E-mail address: zhyxia@hotmail.com (Z. Xia).

https://doi.org/10.1016/j.earscirev.2023.104432
Received 7 October 2022; Received in revised form 13 April 2023; Accepted 16 April 2023
Available online 23 April 2023
0012-8252/© 2023 Elsevier B.V. All rights reserved.

1. Introduction

Stable isotopes of meteoric water are powerful tracers for the atmospheric water cycle (Dansgaard, 1964; Gat, 1996). Globally, the hydrogen and oxygen isotope compositions of precipitation, δ^2H and $\delta^{18}O$,[1] vary in a ratio of about 8:1, reflecting the dominance of mass-dependent equilibrium fractionation in the atmospheric water cycle wherein heavy isotope species are preferentially removed from water vapor by continuous cooling and distillation (Dansgaard, 1964). The second-order deuterium excess (d-excess) parameter, defined as $\delta^2H - 8 \times \delta^{18}O$, was developed to relate the small deviation from the linear δ^2H–$\delta^{18}O$ reference relationship to the component of kinetic fractionation and has a global average value of 10‰ (Craig, 1961; Dansgaard, 1964). Variations in precipitation d-excess may result from an array of hydroclimate processes including oceanic evaporation into the unsaturated atmosphere at the moisture source (Merlivat and Jouzel, 1979), terrestrial moisture recycling in vapor transport (Gat and Matsui, 1991; Gat et al., 1994), and local raindrop re-evaporation within unsaturated air columns (Stewart, 1975) or snow formation in supersaturated environments (Jouzel and Merlivat, 1984). Overall, precipitation d-excess data provide constraints to fingerprint the vapor source conditions and other regional or local modifications, and aid in a thorough understanding of water cycle dynamics with potential applications in a range of topics. However, until now, an accurate and quantitative interpretation of d-excess data has been challenging as there are multiple fractionation steps in the water cycle (Xia et al., 2022).

Recent advances in high-precision triple oxygen isotope measurements allow for distinguishing the tiny mass-dependent partitioning between ^{17}O and ^{18}O (Barkan and Luz, 2005; Schauer et al., 2016). The excess term of ^{17}O in meteoric water, namely $\Delta'^{17}O$ as recommended by Aron et al. (2021), is defined as: $\delta'^{17}O - 0.528 \times \delta'^{18}O$, with $\delta' = \ln(\delta + 1)$, typically reported in per meg (Meijer and Li, 1998; Miller, 2002; Barkan and Luz, 2007). Here, 0.528 is the reference slope (λ) defined by average meteoric water in the $\delta'^{17}O$ vs. $\delta'^{18}O$ space (Luz and Barkan, 2010), analogous to the slope of 8 in the definition of d-excess. Both theory and experiments indicate that $\delta'^{17}O$ and $\delta'^{18}O$ shift by a ratio of $\theta_{eq} = 0.529$ in equilibrium fractionation of water phase change (Barkan and Luz, 2005) and a ratio of $\theta_{diff} = 0.518$ in kinetic fractionation of water vapor diffusion through the air[2] (Barkan and Luz, 2007). These ratios that describe the power law of mass-dependent partitioning between ^{17}O and ^{18}O can be viewed as constants for the range of Earth's surface temperature (Van Hook, 1968; Landais et al., 2012b; Hellmann and Harvey, 2020). From above, the $\Delta'^{17}O$ represents the deviation from the linear $\delta'^{17}O$–$\delta'^{18}O$ reference relationship primarily related to kinetic fractionation (i.e., $\theta_{diff} = 0.518$ relative to a reference slope of 0.528), analogous to d-excess (Angert et al., 2004; Barkan and Luz, 2007; Luz and Barkan, 2010). In addition to applications in ice core-based paleoclimate reconstructions (Landais et al., 2008; Landais et al., 2018; Steig et al., 2021), the major interest in $\Delta'^{17}O$ arises from the prospect that it can be measured in many oxygen-containing geological materials as a novel proxy to reconstruct the ancient water cycle under different tectonic and climatic conditions (Passey et al., 2014; Chamberlain et al., 2020; Sha et al., 2020; Kelson et al., 2022), whereas the d-excess can rarely be determined except in ice-core records, ancient groundwater, or structurally-bonded water. To this end, there is a need to establish the patterns and drivers of $\Delta'^{17}O$ variations in modern meteoric water from the rapidly growing database of measurements (Aron et al., 2021; Surma et al., 2021; Aron et al., 2023).

First assessments on the applicability of $\Delta'^{17}O$ have pointed out that the $\Delta'^{17}O$ of oceanic evaporation fluxes is only affected by relative humidity (RH) above the ocean surface, and unlike d-excess, is minimally affected by sea surface temperature (SST), due to their different responses to temperature-dependent equilibrium fractionation (Angert et al., 2004; Landais et al., 2008). This distinction implies that these two parameters contain complementary information in tracking moisture source conditions and suggests that combined measurements of d-excess and $\Delta'^{17}O$ in polar ice cores have the potential to provide independent records of oceanic temperature and humidity variations in the past (Angert et al., 2004; Landais et al., 2008; Uemura et al., 2010; Landais et al., 2012b). However, it has also been shown that polar precipitation $\Delta'^{17}O$ is strongly affected by local supersaturation conditions at low temperatures during snow formation, and that $\Delta'^{17}O$ data, when combined with paired d-excess data, are more useful to constrain the elusive microphysics of mixed-phase and ice clouds (Angert et al., 2004; Winkler et al., 2012; Schoenemann et al., 2014). In non-polar regions, studies show continental-scale spatial variations in precipitation $\Delta'^{17}O$ that are likely controlled by region-specific factors, with lower $\Delta'^{17}O$ values linked to raindrop re-evaporation or mixing and higher $\Delta'^{17}O$ values linked to terrestrial moisture recycling (Li et al., 2015; Tian et al., 2019). Other studies have collected daily or monthly precipitation samples at individual sites to establish the seasonal patterns in precipitation $\Delta'^{17}O$ and explore their drivers based on the simple correlation between $\Delta'^{17}O$ and meteorological factors (e.g., Landais et al., 2010; Tian et al., 2018; Uechi and Uemura, 2019; Giménez et al., 2021; He et al., 2021). Recently, Aron et al. (2023) derived an extensive precipitation dataset in the conterminous US and showed a consistent pattern of higher $\Delta'^{17}O$ in winter and lower $\Delta'^{17}O$ in summer.

Despite the progress to date, few studies explore in depth the connection between d-excess and $\Delta'^{17}O$ in non-polar regions where their controls are complex (Landais et al., 2010; Xia, 2023; Aron et al., 2023). Previous studies have found that the positive correlation between paired precipitation d-excess and $\Delta'^{17}O$ data appears to be very weak or non-existent (Li et al., 2015; Tian et al., 2018; Aron et al., 2021; He et al., 2021). From a theoretical perspective, d-excess and $\Delta'^{17}O$ are similar parameters, increasing or decreasing in tandem by kinetic fractionation, a fact that has been well described (Uemura et al., 2008; Landais et al., 2010; Uemura et al., 2010; Li et al., 2015; Surma et al., 2018; Bershaw et al., 2020; Aron et al., 2021). However, much less attention has been placed on their different responses and sensitivities to a combination of equilibrium and kinetic fractionation in each step of the water cycle, which may give rise to distinct variations in precipitation d-excess and $\Delta'^{17}O$ (Risi et al., 2013). Furthermore, both d-excess and $\Delta'^{17}O$ have complex controls because their numerical values measured in precipitation samples are composite signals aggregated by multiple fractionation steps (Xia et al., 2022; Aron et al., 2023).

In this contribution, we use theoretical models to decompose the common and distinct features of variations in d-excess and $\Delta'^{17}O$ that occur in each step of the water cycle (Fig. 1a). Section 2 focuses on oceanic evaporation. Section 3 focuses on condensation (including snow formation), Rayleigh distillation, and vapor mixing. Section 4 focuses on terrestrial moisture recycling and raindrop re-evaporation. We characterize the relationship between the shift in d-excess and the shift in $\Delta'^{17}O$ induced by a particular process, which are denoted as Δ(d-excess) and $\Delta(\Delta'^{17}O)$, respectively, as illustrated in the conceptual diagram Fig. 1b. Kinetic fractionation in simple diffusional transport of water vapor is supposed to result in the ratio of the shift in $\Delta'^{17}O$ to the shift in d-excess, $\Delta(\Delta'^{17}O)/\Delta$(d-excess), of about 1.4 per meg/‰ (Appendix A), based on the diffusivities of different isotope species (Merlivat, 1978;

[1] The δ notation is defined as $\delta = (R_s/R_{std} - 1)$, typically reported in per mille, where R_s and R_{std} are the molar ratio of $^2H/^1H$, $^{17}O/^{16}O$, or $^{18}O/^{16}O$ in the sample and Vienna Standard Mean Ocean Water (VSMOW) standard, respectively. For inter-laboratory comparisons of triple oxygen isotope measurements and in order to account for instrument-specific scale compression effects, $\delta^{18}O$ and $\delta^{17}O$ data are normalized to both VSMOW and Standard Light Antarctic Precipitation (SLAP). Schoenemann et al. (2013) provided a widely accepted framework for data normalization.

[2] The θ notation describes the ratio of mass-dependent fractionation between $^{17}O/^{16}O$ and $^{18}O/^{16}O$ as ${}^{17}\alpha = ({}^{18}\alpha)^{\theta}$ (Angert et al., 2003), where ${}^{17}\alpha$ and ${}^{18}\alpha$ are their fractionation factors, respectively, which can be either equilibrium or kinetic fractionation factor.

Barkan and Luz, 2007). In the atmospheric water cycle, kinetic fractionation occurs in a more complex manner, often in company with equilibrium fractionation, and this ratio becomes variable. A higher ratio indicates a relatively larger magnitude of shift—or a more sensitive response—in $\Delta'^{17}O$ than in d-excess, shown as Scenario 2 compared to Scenario 3 (Fig. 1b). In addition, a large shift in $\Delta'^{17}O$ may occur with a negligible shift in d-excess and a negligible shift in $\Delta'^{17}O$ may occur with a large shift in d-excess, as shown in Scenarios 1 and 4, respectively (Fig. 1b). These four scenarios are examples to illustrate the different responses and sensitivities of d-excess and $\Delta'^{17}O$ that we aim to distinguish, in order to develop an interpretive framework for leveraging the joint information from d-excess and $\Delta'^{17}O$ data in fingerprinting water cycle processes. In Section 5, we conduct a data-model comparison analysis to understand the skill of theoretical models in reproducing the observed patterns in precipitation d-excess and $\Delta'^{17}O$ variations. Finally, in Section 6, we discuss the implications of these new analyses and offer several perspectives on d-excess and $\Delta'^{17}O$.

2. Oceanic evaporation

Surface evaporation from oceans is the ultimate origin of atmospheric water vapor and responsible for the average d-excess value in global precipitation (Dansgaard, 1964; Merlivat and Jouzel, 1979). Changes in evaporation source conditions, including factors like SST, RH above the ocean surface, aerodynamic condition, and the isotopic composition of boundary layer vapor, affect the d-excess of oceanic evaporation fluxes that is transmitted to the free troposphere and then precipitation over continents through vapor transport and condensation (Merlivat and Jouzel, 1979; Johnsen et al., 1989; Pfahl and Sodemann, 2014; Aemisegger and Sjolte, 2018). These controls have been well described by the oceanic evaporation model introduced by Craig and Gordon (1965). In this model, kinetic fractionation occurs in the diffusional transport of water vapor across a laminar layer between the liquid-air interface below and the turbulent atmosphere above. The kinetic fractionation factor can be empirically represented by the ratio of diffusivity (Pfahl and Wernli, 2009). The isotopic composition of the oceanic evaporation flux ($^{X}\delta_{oe}$) follows:

$$^{X}\delta_{oe}(‰) = \frac{\left(\frac{^{X}D'}{^{X}D}\right)^{m}\left[\left(^{X}\alpha_{eq}^{l-v}\right)^{-1}\left(^{X}\delta_{o}+1000\right)-\left(\frac{h_s}{100}\right)\left(^{X}\delta_{a}+1000\right)\right]}{1-\left(\frac{h_s}{100}\right)}-1000, \quad (1)$$

where $^{X}D'/\,^{X}D$ is the ratio of diffusion coefficients of the heavy over the light isotope species, m is the aerodynamic exponent, $^{X}\alpha_{eq}^{l-v}$ is the liquid-vapor equilibrium fractionation factor at SST (>1), $^{X}\delta_{o}$ and $^{X}\delta_{a}$ are the isotopic compositions of ocean water (assumed as 0‰, but available data from Luz and Barkan (2010) indicate slightly negative $\Delta'^{17}O$ values in modern ocean water) and boundary layer vapor (in ‰), respectively, and h_s is the oceanic RH (in %; "oceanic" stresses that RH is normalized to saturation vapor pressure at SST). In this paper, X denotes the individual heavy isotope species (2 for ^{2}H, 18 for ^{18}O, 17 for ^{17}O).

For simplicity, the closure assumption is often applied to the model,

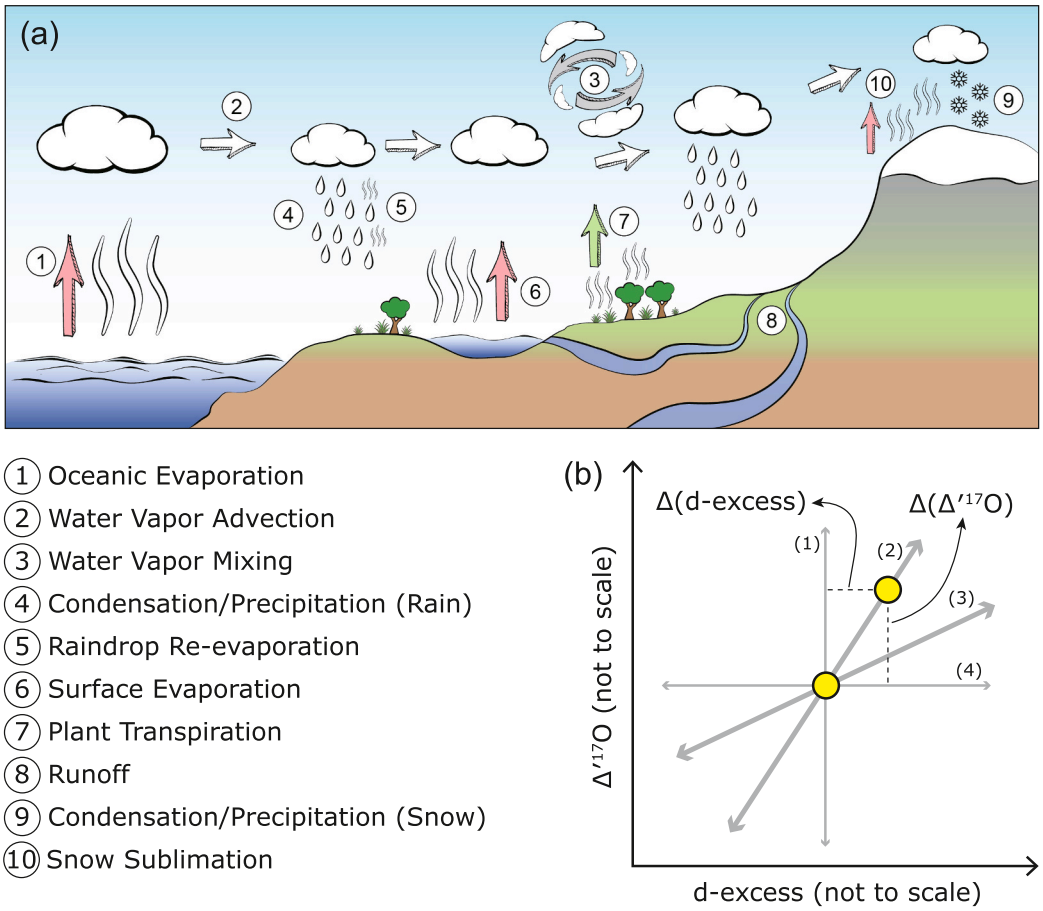

Fig. 1. (a) The schematic of water cycle processes that are relevant for understanding d-excess and $\Delta'^{17}O$ behavior. (b) The conceptual diagram on the relationship between the shifts in d-excess and $\Delta'^{17}O$ (yellow dots are the isotopic compositions before and after the shifts). Four scenarios are considered: (1)—a large shift in $\Delta'^{17}O$ with a negligible shift in d-excess; (2)—shifts in both $\Delta'^{17}O$ and d-excess; (3)—shifts in both $\Delta'^{17}O$ and d-excess but with a lower slope compared to (2); and (4)—a large shift in d-excess with a negligible shift in $\Delta'^{17}O$. These shifts are denoted as Δ(d-excess) and Δ($\Delta'^{17}O$). (For interpretation of the references to color in this figure legend, the reader is referred to the web version of this article.)

meaning that boundary layer vapor is only supplied by evaporation fluxes (Merlivat and Jouzel, 1979; Aemisegger and Sjolte, 2018), i.e., ${}^{X}\delta_{oe} = {}^{X}\delta_{a}$. Then, the following expression is derived:

$$ {}^{X}\delta_{oe}\,(‰) = \frac{\left({}^{X}\alpha_{eq}^{l-v}\right)^{-1}\left(\frac{{}^{X}D'}{{}^{X}D}\right)^{m}\left({}^{X}\delta_{o}+1000\right)}{1-\left(\frac{h_s}{100}\right)\left[1-\left(\frac{{}^{X}D'}{{}^{X}D}\right)^{m}\right]} - 1000. \quad (2) $$

The values of ${}^{X}\alpha_{eq}^{l-v}$ and ${}^{X}D'/{}^{X}D$ are provided in Appendices A and B. The aerodynamic exponent can be expressed as $m \approx n \times \Theta$, where n expresses the ratio of diffusional over turbulent transport in the laminar layer and Θ expresses the extra effect of turbulence in the turbulent atmosphere (Gat, 1996; Pfahl and Wernli, 2009). For open oceans, $\Theta = 0.5$ and $n = 0.5$ are reasonable values (Gat, 1996), so that $m = 0.25$, but there is no consensus. Other studies have determined the empirical values of $({}^{X}D'/{}^{X}D)^{m}$, referred to as the kinetic fractionation factor of evaporation, without explicitly calculating m values, although back-calculated m values are close to 0.25 (Merlivat and Jouzel, 1979; Pfahl and Wernli, 2009; Uemura et al., 2010). Qualitatively, a higher or lower m value can be thought of as a smoother (low wind speed) or rougher (high wind speed) surface regime above oceans, respectively (Merlivat and Jouzel, 1979; Benetti et al., 2014).

Here, given a range of SST from 0 °C to 30 °C and oceanic RH from 20% to 110%, Eq. (2) is used to calculate the d-excess for each combination of SST and oceanic RH, and then a multiple linear regression is derived as: d-excess (‰) = $-0.50 \times h_s + 0.35 \times$ SST $+ 42$. This formulation suggests that both SST and oceanic RH affect the d-excess of oceanic evaporation fluxes if other m values and the validity of the closure assumption are not considered. This is the basis for the use of d-excess as a proxy for moisture source regions and conditions on long timescales in ice core-based paleoclimate reconstructions, in which most studies interpret d-excess records as reflecting SST variations at the moisture source, considering that oceanic RH is found to vary little in

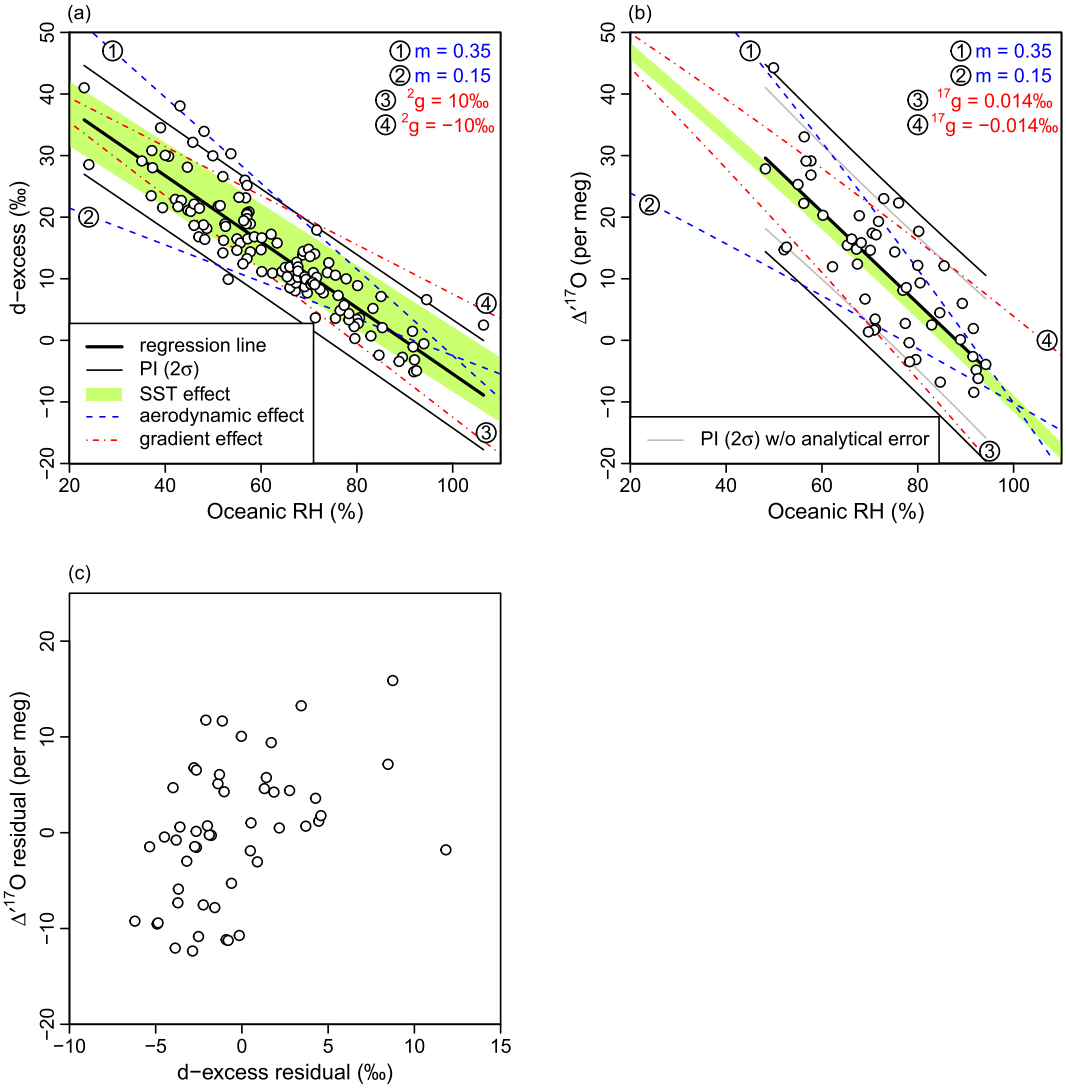

Fig. 2. The effect of oceanic evaporation. (a) The scatter plot between oceanic vapor d-excess and oceanic RH based on data from three studies compiled by Pfahl and Sodemann (2014) with their ordinary least square regression (thick black line) line and 2σ prediction interval (thin black lines). These data are compared with model-based predictions, including the green bar that shows the range of variability when SST is between 0 °C and 30 °C, blue dashed lines when aerodynamic exponent m is 0.15 or 0.35 (SST = 15 °C), and red dashed lines when the d-excess of the boundary layer vapor is assumed to be 10‰ higher or lower than that of the oceanic evaporation flux (SST = 15 °C). (b) The scatter plot between oceanic vapor $\Delta'^{17}O$ and oceanic RH from data from Uemura et al. (2010) after rescaling according to Li et al. (2015). The gray lines show the 2σ prediction interval after the analytical error is discounted using inverse error propagation. Other information is the same as (a) except those red dashed lines, which result from assuming that the $\Delta'^{17}O$ of the boundary layer vapor is 14 per meg high or lower than the oceanic evaporation flux. (c) The scatter plot between regression residuals of paired oceanic vapor $\Delta'^{17}O$ and d-excess data from the Southern Ocean (Uemura et al., 2008; Uemura et al., 2010). (For interpretation of the references to color in this figure legend, the reader is referred to the web version of this article.)

simulations of coupled general circulation models (GCMs) (Vimeux et al., 1999; Stenni et al., 2001; Markle et al., 2017).

Recently, Pfahl and Sodemann (2014) used observational data to argue that oceanic RH is the main driver of oceanic vapor d-excess, at least on seasonal timescales with an empirical linear relationship as: d-excess $= -0.54 \times h_s + 48.2$ (Fig. 2a). Their compiled data indicate that SST, which features smaller variability on synoptic and seasonal timescales compared to oceanic RH, does not affect the d-excess of oceanic evaporation fluxes as strongly as oceanic RH. We also find that including SST as an independent variable increases the coefficient of determination very little compared to using oceanic RH only (R^2 from 0.80 to 0.81). The linear regression between d-excess and oceanic RH from observations is in good agreement with the space of model predictions based on the closure assumption, although the scattering of data points (as indicated by the 2σ prediction interval of the regression line) is wider than the d-excess variability driven by the SST effect alone (Fig. 2a). The formulation of a simple linear relationship between d-excess and oceanic RH has been supported by other more extensive studies on stable isotopes of oceanic vapor with slight differences in regression coefficient (Benetti et al., 2014; Steen-Larsen et al., 2014). However, a more recent study that made use of a large observational dataset of water vapor over the Atlantic Ocean has derived a multiple linear regression for d-excess that includes both SST and oceanic RH as the independent variables (Bonne et al., 2019). A new analysis of global precipitation dataset also found that the diagnosed moisture source SST contributes to a fair portion of variability in precipitation d-excess (Xia, 2023). These together suggest that the role of SST cannot be ignored.

For $\Delta'^{17}O$ of oceanic evaporation fluxes, the same multiple linear regression is derived from Eq. (2) as: $\Delta'^{17}O = -0.72 \times h_s + 0.09 \times SST + 60$. The low regression coefficient for SST indicates a very weak sensitivity of $\Delta'^{17}O$ to SST, with a difference of 30 °C in SST introducing only a < 3 per meg change in $\Delta'^{17}O$. Currently, measurements of oceanic vapor $\Delta'^{17}O$ are sparse and only available in one study that still has covered a large latitudinal gradient across the Southern Ocean and has paired d-excess data (Uemura et al., 2008; Uemura et al., 2010). Their results also suggest that an empirical linear relationship can be established between oceanic vapor $\Delta'^{17}O$ and oceanic RH as: $\Delta'^{17}O = -0.74 \times h_s + 65.3$ (Fig. 2b). Just like for d-excess, the linear regression between $\Delta'^{17}O$ and oceanic RH in observations is in good agreement with the space of model predictions based on the closure assumption, i.e., Eq. (2). However, the regression has a wide 2σ prediction interval at about ± 15 per meg, or ± 12 per meg if the reported analytical error of 5 per meg (1σ) is discounted using inverse error propagation (Fig. 2b), suggesting that a large proportion of $\Delta'^{17}O$ variability is unexplained by oceanic RH and is unlikely driven by SST.

From above, both models and observations at least strongly support that the d-excess and $\Delta'^{17}O$ of oceanic evaporation fluxes have a common response to and are linearly correlated with oceanic RH at a scaling relationship of about 1.33 (0.74/0.54) per meg/‰. Still, there are other secondary mechanisms responsible for the variability in both d-excess and $\Delta'^{17}O$ as reflected by the scattering of data points in the regression against oceanic RH. A further analysis reveals that regression residuals of d-excess and $\Delta'^{17}O$ data from the paired isotopic measurements of oceanic vapor from the Southern Ocean exhibit a weak positive correlation ($R^2 = 0.19$, $p = 10^{-3}$; Fig. 2c), suggesting that there exist common drivers introducing additional shifts in $\Delta'^{17}O$ and d-excess simultaneously that remains unexplained by oceanic RH alone.

From a theoretical consideration, the isotopic composition of oceanic evaporation fluxes is additionally affected by the aerodynamic condition over oceans and the incorporation of water vapor from other sources into the boundary layer locally violating the closure assumption. To explore their individual effects on d-excess and $\Delta'^{17}O$ of oceanic evaporation fluxes, we impose the value of aerodynamic exponent m to be 0.15 or 0.35 to represent a relatively weaker or stronger molecular diffusion (Pfahl and Wernli, 2009), termed as the aerodynamic effect. We also extend the closure assumption by considering different isotopic compositions of boundary layer vapor that modulate isotopic gradients and thus diffusional transport of isotope species at the site of evaporation (Aemisegger and Sjolte, 2018), termed as the gradient effect. This gradient effect is incorporated into Eq. (1) with ${}^X\delta_a = {}^X\delta_{oe} + {}^Xg$ and the following is derived:

$$ {}^X\delta_{oe}\ (‰) = \frac{\left({}^X\alpha_{eq}^{l-v}\right)^{-1}\left(\frac{{}^X D'}{{}^X D}\right)^m\left({}^X\delta_o + 1000\right) - \left(\frac{h_s}{100}\right)\left(\frac{{}^X D'}{{}^X D}\right)^m {}^Xg}{1 - \left(\frac{h_s}{100}\right)\left[1 - \left(\frac{{}^X D'}{{}^X D}\right)^m\right]} - 1000, \qquad (3) $$

where ${}^Xg$ is the instantaneous isotopic offset between boundary layer vapor and oceanic evaporation fluxes for heavy isotope species X (in ‰). If ${}^Xg > 0$‰, the boundary layer vapor has a relatively higher δ-value than the oceanic evaporation flux rather than being equal. This feedback results in a relatively lower δ-value of the oceanic evaporation flux compared to the case of the closure assumption. We apply Eq. (3) by setting ${}^2g = 10$‰ or − 10‰ and ${}^{17}g = 0.014$‰ or − 0.014‰, meaning that there is a positive or negative gradient of 10‰ for d-excess and 14 per meg for $\Delta'^{17}O$ when the evaporation flux diffuses upward into the free troposphere, while the closure assumption is maintained for $\delta^{18}O$. The violation of the closure assumption, in reality, is often related to phenomena such as subsidence or lateral advection of water vapor and affects $\delta^{18}O$ as well (Jouzel and Koster, 1996; Kurita, 2013; Benetti et al., 2015), but we note that our purpose is to explore the common driver responsible for both $\Delta'^{17}O$ and d-excess variability that remains unexplained by the oceanic RH alone.

The oceanic evaporation model is run with added aerodynamic and gradient effects for variable oceanic RH and at a constant SST at 15 °C. The results are plotted in Fig. 2a and b as dashed lines. Certainly, different values of aerodynamic exponent m (blue dashed lines) and isotopic gradient ${}^Xg$ (red dashed lines) shift d-excess and $\Delta'^{17}O$ compared to the case of $m = 0.25$ and ${}^2g = {}^{17}g = 0$‰ (solid black lines). Notably, d-excess and $\Delta'^{17}O$ have a higher sensitivity to the aerodynamic effect at lower oceanic RH and a higher sensitivity to the gradient effect at higher oceanic RH. These two effects together have largely encompassed the distribution of measured d-excess and $\Delta'^{17}O$ data. Accordingly, if the scattering of data points is indeed the result of variability induced by aerodynamic and gradient effects, their actual magnitudes in natural observations are likely smaller than what we arbitrarily imposed in the model.

With these simple tests of modified models, we demonstrate that both the aerodynamic conditions and isotopic gradients at the boundary layer are important drivers of coupled d-excess and $\Delta'^{17}O$ variability in oceanic evaporation fluxes that cannot be explained by oceanic RH alone, at least on short timescales. In theory, these two mechanisms may explain the weak positive correlation between the regression residuals of d-excess and $\Delta'^{17}O$ in observational data (Fig. 2c). Specifically, the relatively higher d-excess and $\Delta'^{17}O$ of oceanic evaporation fluxes at the same oceanic RH may result from a stronger molecular diffusion regime (higher m values) or the case that d-excess and $\Delta'^{17}O$ in the boundary layer vapor are both relatively lower. Identifying these additional mechanisms is relevant for understanding the complementary nature of these two parameters in reflecting moisture source conditions. While it is theoretically possible to distinguish the independent effect of SST and oceanic RH at the moisture source based on the contrasting sensitivity of d-excess and $\Delta'^{17}O$ to temperature-dependent equilibrium fractionation (Angert et al., 2004; Xia, 2023), we suggest that it is necessary for such applications to evaluate whether the independent SST effect in an individual pair of d-excess and $\Delta'^{17}O$ data has been overprinted by the aerodynamic and gradient effects that are highly variable in nature on short timescales (Aemisegger and Sjolte, 2018). Together, our analysis stresses that oceanic vapor d-excess and $\Delta'^{17}O$ have multiple common drivers and reflect largely similar moisture source information, beyond their theoretically different responses to SST.

3. Condensation, Rayleigh distillation, and mixing

The response of d-excess and $\Delta'^{17}O$ to oceanic evaporation provides a mechanism to link their signals preserved in continental precipitation with oceanic moisture source regions and conditions. An assumption for this application is that isotopic fractionation during condensation and distillation of oceanic vapor across climate gradients affects the first-order δ-values in precipitation but does not strongly modify the signals of second-order d-excess and $\Delta'^{17}O$ that have been initially set at the oceanic moisture source (Merlivat and Jouzel, 1979). In this section, we evaluate the validity and limitation of this assumption based on the Rayleigh distillation model with additional consideration of its interaction with vapor mixing.

3.1. Condensation and Rayleigh distillation

The Rayleigh distillation model describes the change in the isotopic composition of water vapor ($^X\delta_v$) with condensate relatively enriched in heavy isotope species being continuously removed from the vapor phase as (Dansgaard, 1964):

$$^X\delta_v\ (‰) = \left(^X\delta_{v,0} + 1000\right) f^{^X\alpha_{eff}-1} - 1000, \tag{4}$$

where $^X\delta_{v,0}$ is the initial isotopic composition of water vapor (in ‰), f is the fraction of remaining vapor, and $^X\alpha_{eff}$ is the effective fractionation factor between condensate and vapor (>1). The equations for deriving $^X\alpha_{eff}$ are listed in Appendix B. Briefly, ice-vapor fractionation that contains a kinetic effect due to supersaturation of water vapor over ice starts to replace liquid-vapor fractionation once the condensation temperature (T_d) is lower than 0 °C in mixed-phase conditions until −23 °C when the condensate is purely ice (Dütsch et al., 2017). This setup of fractionation factors is intended to simplify the complex precipitation formation mechanisms in the real world. For example, pure liquid-vapor fractionation may further extend to temperatures <0 °C in which ice condensate is formed by direct freezing of supercooled liquid in strong updrafts (Lohmann et al., 2016; Graf et al., 2019; Surma et al., 2021).

Rayleigh distillation is often required to follow a certain temperature gradient to allow continuous removal of condensate, meaning that f is controlled by T_d. Their relationship can be approximated by the temperature-dependent saturation vapor pressure as (Bolton, 1980):

$$f = exp\left(\frac{17.67T_d}{T_d + 243.5} - \frac{17.67T_{d,0}}{T_{d,0} + 243.5}\right), \tag{5}$$

where $T_{d,0}$ is the initial T_d (both in °C). Because both f and $^X\alpha_{eff}$ vary with T_d, Eq. (4) should be computed in discrete steps for a given temperature gradient, each step incorporating updated f and $^X\alpha_{eff}$ values. The isotopic composition of precipitation ($^X\delta_p$) at each step of Rayleigh distillation is calculated as:

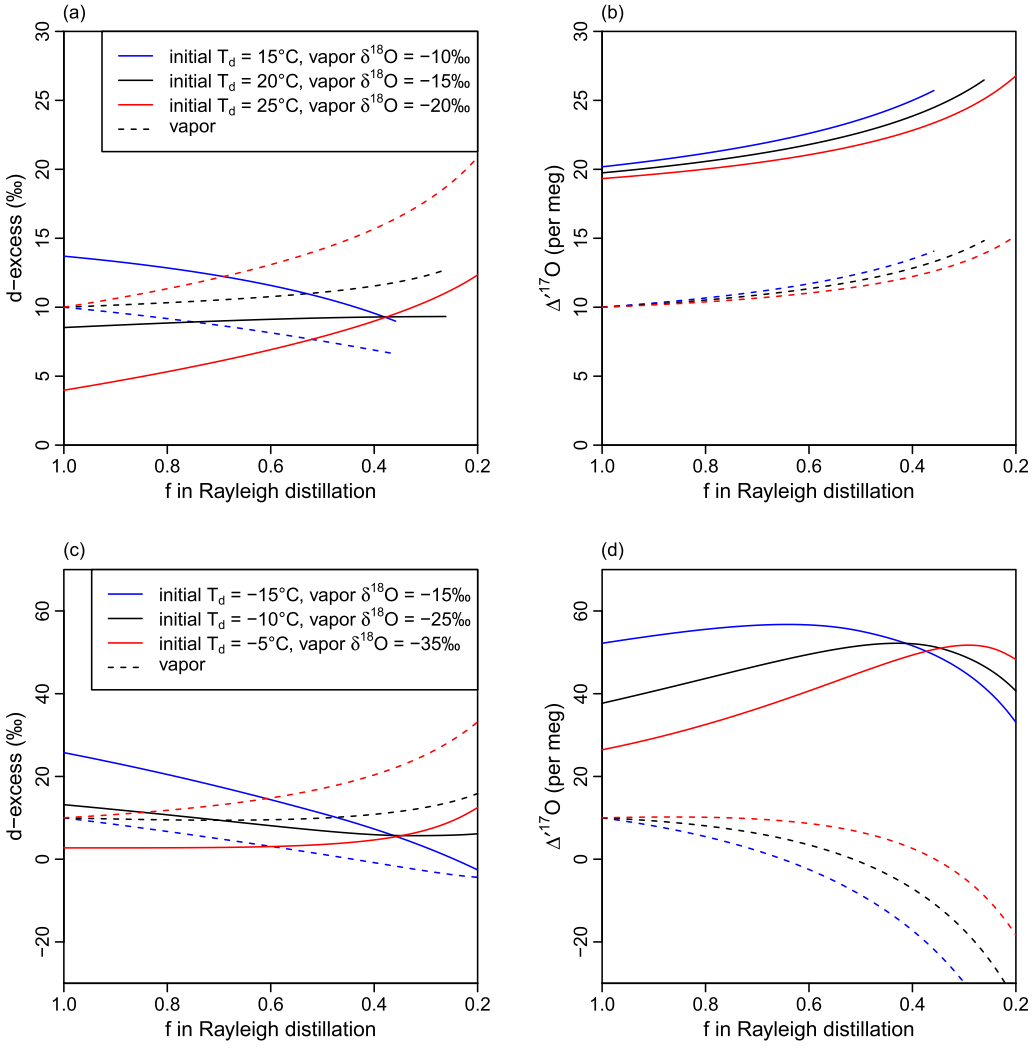

Fig. 3. Rayleigh distillation curves for d-excess (a, c) and $\Delta'^{17}O$ (b, d) from three simulations of different initial conditions when condensate is liquid (a, b) and when condensate has ice (c, d). Solid lines denote precipitation and dashed lines denote water vapor.

$$^{X}\delta_p\ (‰) = \left(^{X}\delta_v + 1000\right)^{X}\alpha_{eff} - 1000. \quad (6)$$

Our previous study explored the d-excess variations in Rayleigh distillation and provided two caveats about d-excess that are still important in non-polar regions (Xia et al., 2022). First, precipitation, even in liquid phase in equilibrium with water vapor, may have a large shift in d-excess from the co-existing vapor phase due to the fractionation during condensation. Second, the d-excess of water vapor is accordingly modified in response to the progressive removal of condensate, which in turn controls the d-excess of precipitation at later stages of Rayleigh distillation. That is, the d-excess is not conservative during condensation nor in Rayleigh distillation. The direction and magnitude of these shifts are controlled by the balance of two factors: T_d and vapor $\delta^{18}O$ (Dütsch et al., 2017).

To demonstrate the non-conservative nature of d-excess, we show three Rayleigh distillation simulations in which condensate is precipitated as liquid only (Fig. 3a) and in which condensate is in partially or fully precipitated as ice (Fig. 3c). All Rayleigh distillation curves differ in their initial T_d and vapor $\delta^{18}O$ but have the same initial vapor d-excess of 10‰. In the case where relatively low T_d is combined with high vapor $\delta^{18}O$, precipitation d-excess is higher than vapor d-excess, and both decrease with progressive distillation (blue lines). An opposite pattern is observed when relatively high T_d is combined with low vapor $\delta^{18}O$ (red lines). These above two cases may characterize the initial conditions prevailing in cold and warm seasons, respectively (Xia et al., 2022). For the case where intermediate T_d and vapor $\delta^{18}O$ are combined, a near-conservative behavior in d-excess is shown (black lines). Another interesting feature is that regardless of the non-conservative behavior in d-excess under different initial conditions, three precipitation d-excess curves converge to the same value (9‰ when condensate is precipitated as liquid only and 5‰ when condensate is partially or fully precipitated as ice) as f decreases to about 0.35–0.4 (Fig. 3a and c). Qualitatively, this feature suggests that as condensate with higher or lower d-excess than vapor is continuously removed, the d-excess of remaining vapor will accordingly decrease or increase in pace until it reaches a composition that produces condensate with the d-excess value close to that in initial vapor ($f = 1$), always at the similar degree of distillation. Mathematically, the f value at which Rayleigh distillation curves converge (f_c) can be derived by combining Eqs. (4) and (6) and assuming $^{X}\delta_p = {}^{X}\delta_{v,0}$ as:

$$f_c = \left(^{X}\alpha_{eff}\right)^{\frac{1}{1-{}^{X}\alpha_{eff}}}. \quad (7)$$

The value of f_c is not sensitive to $^{X}\alpha_{eff}$. As an example, when $T_d = 20$ °C, we have $^{2}\alpha_{eff} = 1.0850$ and $^{18}\alpha_{eff} = 1.0098$. These yield f_c values of 0.370 and 0.383, respectively. Since d-excess is a linear combination of δ^2H and $\delta^{18}O$, these results explain our finding that precipitation approaches the d-excess value of initial vapor when f is about 0.35–0.4.

For $\Delta'^{17}O$, under the same simulations of Rayleigh distillation starting with the initial vapor $\Delta'^{17}O$ of 10 per meg, there are different non-conservative behaviors compared to d-excess. When condensate is precipitated as liquid only (Fig. 3b), precipitation $\Delta'^{17}O$ is about 10 per meg higher than vapor $\Delta'^{17}O$, and both increase very slightly with progressive distillation by 5 per meg until T_d decreases to 0 °C, with very little sensitivity to initial conditions. This 10 per meg shift between precipitation and vapor can be calculated from Eq. (A2) and is itself related to the definition of $\Delta'^{17}O$ relative to a reference slope of 0.528, which is lower than the exponent of mass-dependent equilibrium fractionation $\theta_{eq} = 0.529$ (Angert et al., 2004; Barkan and Luz, 2005; Aron et al., 2021). The increase in vapor $\Delta'^{17}O$ throughout Rayleigh distillation may seem counter-intuitive as condensate with higher $\Delta'^{17}O$ is continuously removed, but it is important to note that $\Delta'^{17}O$ is defined based on the logarithmic (non-linear) δ' notation. When condensate is partially or fully precipitated as ice (Fig. 3d), the shift between precipitation and vapor $\Delta'^{17}O$ becomes much higher than 10 per meg, since supersaturation of water vapor over ice at low temperatures induces diffusional transport of water vapor that favors the partitioning of lighter ^{17}O into condensate over ^{18}O. As a result, precipitation $\Delta'^{17}O$ shows an increasing trend at earlier stages of distillation and then transitions into a decreasing trend when distillation proceeds to later stages with lower f (Fig. 3d). This transition indicates the point at which the progressively decreased vapor $\Delta'^{17}O$ eventually outpaces the higher condensate $\Delta'^{17}O$ throughout Rayleigh distillation. Prior to this point (higher f), precipitation $\Delta'^{17}O$ and $\delta^{18}O$ have negative correlations as found in snow over Greenland and West Antarctica, whereas beyond this point (lower f), precipitation $\Delta'^{17}O$ and $\delta^{18}O$ shift to positive correlations as found in snow over much colder East Antarctica (Landais et al., 2012b; Schoenemann and Steig, 2016). This finding differs from the recent review by Aron et al. (2021) who simplistically described supersaturation as a process that leads to decreasing precipitation $\Delta'^{17}O$. Still, these precipitation $\Delta'^{17}O$ curves converge to the same value when f is about 0.35–0.4, a similar feature as d-excess, but this value is about 40 per meg higher than initial vapor $\Delta'^{17}O$ (Fig. 3d).

These Rayleigh distillation simulations are intended to serve as examples of the non-conservative behaviors in d-excess and $\Delta'^{17}O$. Specifically, we show the direction and magnitude of their instantaneous shifts during condensation from vapor to precipitation and their gradual shifts in precipitation throughout the progress of Rayleigh distillation, which hereafter are termed as the 1st and 2nd type of non-conservative behavior, respectively.

To demonstrate the impact of non-conservative behaviors on the relationship between d-excess and $\Delta'^{17}O$ in precipitation, we additionally create more such Rayleigh distillation simulations using the combination of a wide range of initial T_d and vapor $\delta^{18}O$. Rather than showing Rayleigh distillation curves as above, we present the shifts of d-excess and $\Delta'^{17}O$ in precipitation relative to initial vapor, namely the Δ(d-excess) and $\Delta(\Delta'^{17}O)$, under different initial T_d and vapor $\delta^{18}O$ in contour lines at different f values, separately for initial $T_d > 0$ °C (Fig. 4a and b) and initial $T_d < 0$ °C (Fig. 5a and b). The contour lines of Rayleigh $f = 1$ thus represent the 1st type of non-conservative behavior and other contour lines represent the 2nd type of non-conservative behavior. These plots reproduce the key features we have previously identified from selective Rayleigh distillation curves in Fig. 3 and provide a wider context regarding the effects of initial conditions and distillation stages on precipitation d-excess and $\Delta'^{17}O$. For example, the sloping contours in Figs. 4a and 5a indicate that precipitation d-excess is controlled by the balance between T_d and vapor $\delta^{18}O$, while the vertical contours in Figs. 4b and 5b indicate that precipitation $\Delta'^{17}O$ is not affected by vapor $\delta^{18}O$. We note that in plots of initial $T_d > 0$ °C (Fig. 4a and b), when initial T_d is too low, vapor requires being cooled to <0 °C in order to have a sufficient degree of distillation. These situations are not considered so that fractionation is exclusively between liquid and vapor.

Next, we focus on the area plot between paired $\Delta(\Delta'^{17}O)$ and Δ(d-excess) to understand the different responses of precipitation d-excess and $\Delta'^{17}O$ to condensation and Rayleigh distillation. When initial $T_d > 0$ °C and condensate is liquid only (Fig. 4c), the area plot shows an elongated shape for $f = 1$, covering a range of −10‰ to >10‰ for Δ(d-excess) and 9 to 12 per meg for $\Delta(\Delta'^{17}O)$, but the shape becomes much narrower for Δ(d-excess) for $f = 0.4$. This area plot highlights that precipitation $\Delta'^{17}O$ is insensitive to initial conditions and distillation stages, while precipitation d-excess is highly sensitive to initial conditions when f is high. For the case of initial $T_d < 0$ °C and condensate has ice (Fig. 5c), the area plot between $\Delta(\Delta'^{17}O)$ and Δ(d-excess) shows a somewhat quadrilateral shape for $f = 1$, covering a > 20‰ range for Δ(d-excess) and a > 40 per meg range for $\Delta(\Delta'^{17}O)$. This suggests that progressive distillation of water vapor with the same d-excess and $\Delta'^{17}O$ values may result in a wide range of possible d-excess and $\Delta'^{17}O$ combinations in precipitation, which is caused by different initial T_d and vapor $\delta^{18}O$. This shuffling of both d-excess and $\Delta'^{17}O$ through condensation may lead to a pervasive and strong decoupling between d-excess and $\Delta'^{17}O$ in precipitation. However, if water vapor has undergone a higher degree of distillation to about $f = 0.4$, this shuffling effect is reduced as shown by the much narrower area occupied in the plot. At

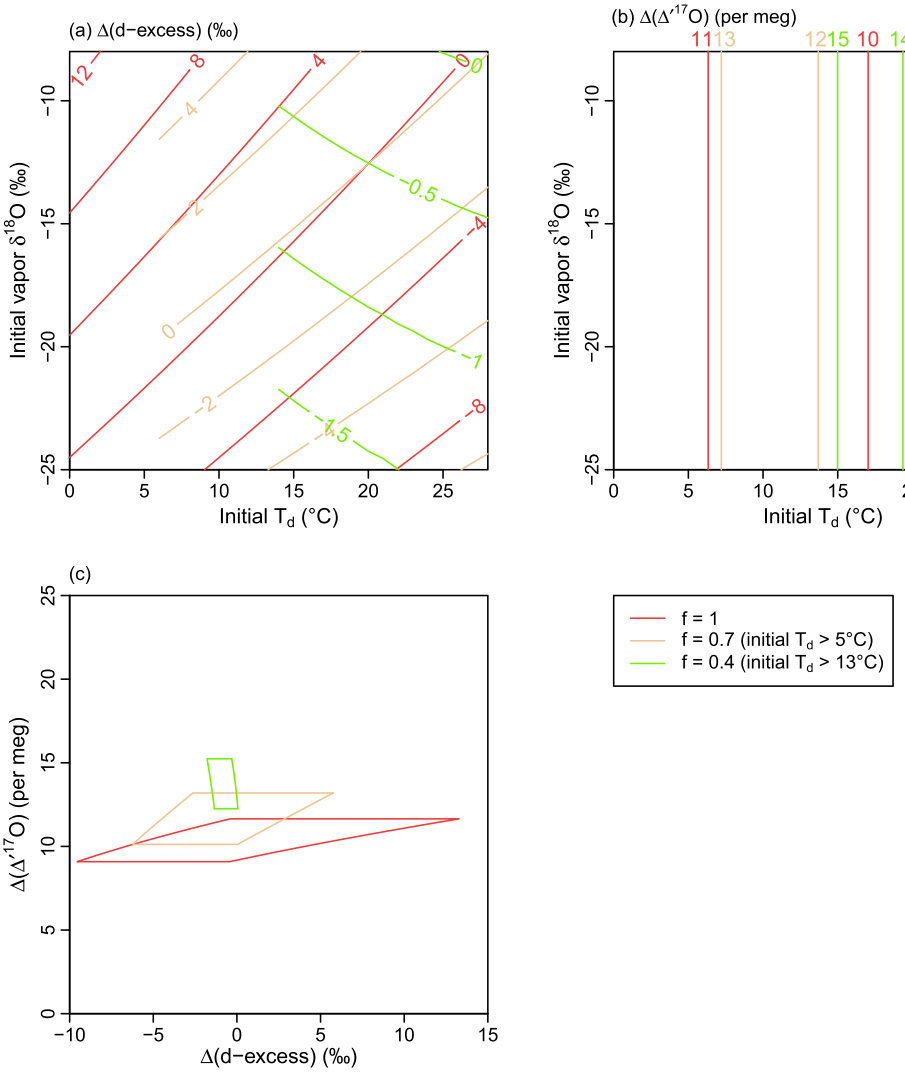

Fig. 4. The effects of initial conditions and distillation stages in Rayleigh distillation for initial $T_d > 0$ °C. (a) Shifts in precipitation d-excess from initial vapor d-excess (10‰), i.e., Δ(d-excess), under different initial T_d and vapor $\delta^{18}O$ are shown as contour lines at different f values. (b) Similar to (a) but for shifts in precipitation $\Delta'^{17}O$ from initial vapor $\Delta'^{17}O$ (10 per meg), i.e., $\Delta(\Delta'^{17}O)$. (c) The area between paired $\Delta(\Delta'^{17}O)$ and Δ(d-excess) at different f values given the range of initial conditions as in (a) and (b).

this stage of distillation, both the d-excess and $\Delta'^{17}O$ of precipitation faithfully reflect the d-excess and $\Delta'^{17}O$ of water vapor after adjusting the Δ(d-excess) and $\Delta(\Delta'^{17}O)$ values of around −5‰ and 40 per meg. As distillation proceeds further to $f = 0.2$, their decoupling reappears.

Finally, the Rayleigh distillation analysis that involves ice condensation at low T_d is based on a particular set of parameterizations for mixed-phase and ice cloud conditions (Appendix B), whereas there is no consensus about this parameterization with other different sets being used in different studies (Landais et al., 2008; Schoenemann et al., 2014; Schoenemann and Steig, 2016). To this end, we additionally test the effects of parameterization in ice-vapor fractionation by assigning the transition temperature between liquid and mixed-phase clouds and between mixed-phase and ice clouds a random value from −10 °C to 0 °C and from −40 °C to −23 °C, respectively, and the supersaturation parameter λ a random value from 0.002 to 0.006 (see Appendix B). We find that our previous findings are robust over different parameterizations except for the fact that the exact value of precipitation $\Delta'^{17}O$ is more sensitive to different parameterizations than precipitation d-excess. This is shown in Fig. S2 where we plot the standard deviation (1σ) of d-excess and $\Delta'^{17}O$ in precipitation from 10^6 realizations of Monte Carlo random parametrizations. This finding is in line with previous studies suggesting that $\Delta'^{17}O$ is highly sensitive to the occurrence of kinetic fractionation during ice formation under supersaturation conditions (Angert et al., 2004; Winkler et al., 2012; Schoenemann et al., 2014).

In this subsection, we have conducted a thorough investigation of variability in precipitation d-excess and $\Delta'^{17}O$ by means of the classic Rayleigh distillation model. Although the same model has been widely utilized to reproduce the spatiotemporal variations of d-excess and, more recently, $\Delta'^{17}O$ in polar snow after model tuning (Johnsen et al., 1989; Petit et al., 1991; Landais et al., 2008; Landais et al., 2012a; Landais et al., 2012b; Winkler et al., 2012; Pang et al., 2015), our new analysis stresses the contrasting non-conservative behaviors of d-excess and $\Delta'^{17}O$ that may overprint source vapor signals and shuffle their scaled relationship established in oceanic evaporation, in particular when the degree of distillation is small (with relatively high δ-values in precipitation). These non-conservative behaviors in nature reflect different responses to equilibrium fractionation. Even when condensation involves ice and the non-conservative behavior results from a combination of equilibrium and kinetic fractionation, it is still the different response to ice-vapor equilibrium fractionation that directly invokes contrasting non-conservative behaviors and the decoupling between d-excess and $\Delta'^{17}O$ during condensation (as the kinetic effect due to supersaturation alone should affect d-excess and $\Delta'^{17}O$ proportionally, see Appendix A).

3.2. Mixing

A limitation of the Rayleigh distillation model in Section 3.1 is that it describes the isotopic evolution of water vapor from a single source, but

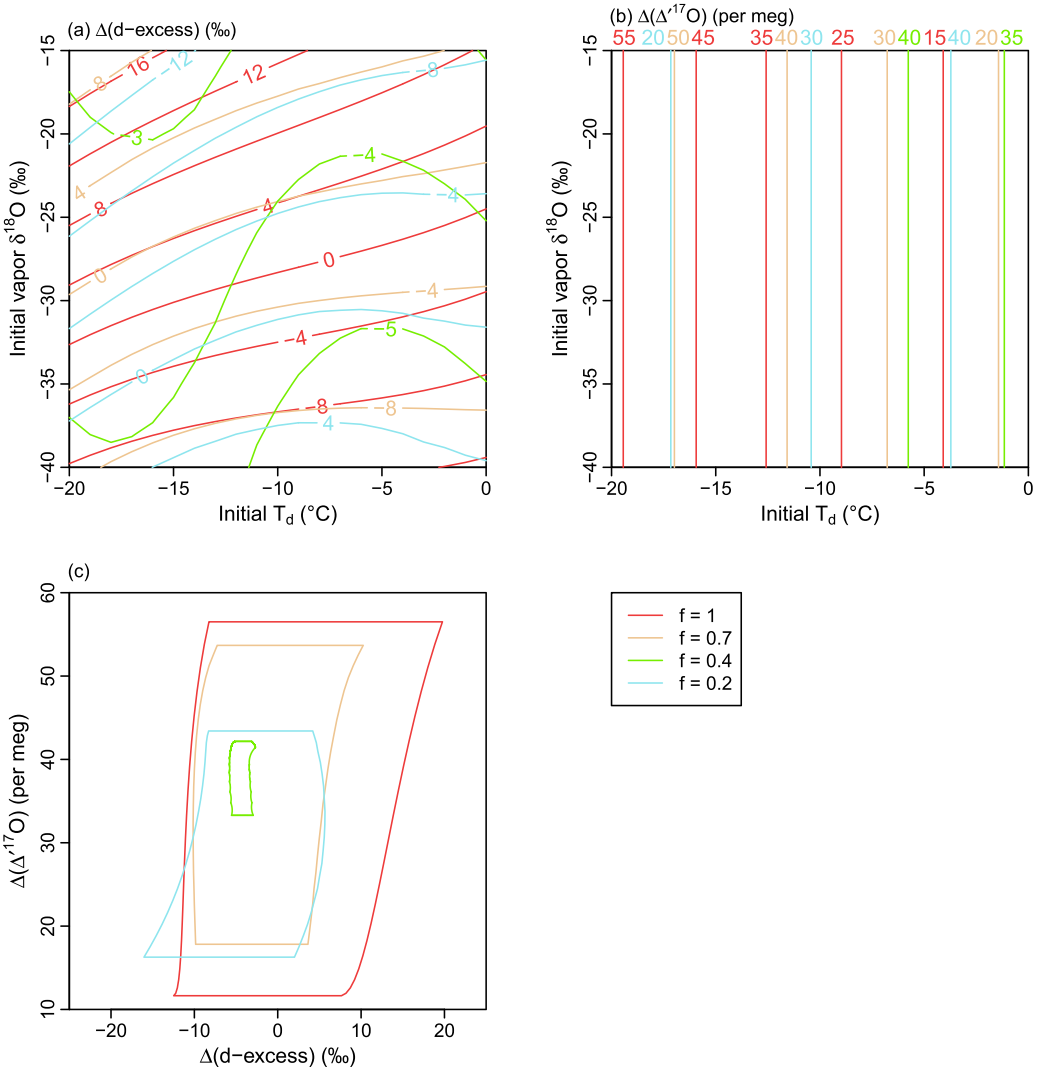

Fig. 5. Similar to Fig. 4 but for initial $T_d < 0$ °C (kinetic effect due to supersaturation of water vapor over ice is incorporated).

in reality, vapor mixing frequently occurs in company with vapor transport and distillation. It is known that vapor mixing affects $\Delta'^{17}O$ differently from d-excess due to its definition on the logarithmic (non-linear) δ' notation (Li et al., 2015; Aron et al., 2021; Leuenberger and Ranjan, 2021). When two water bodies are mixed, their mixture has a $\Delta'^{17}O$ value lower than their mass-weighted arithmetic mean. If the difference in $\delta^{18}O$ between two water bodies is larger, there is a larger deviation of mixture $\Delta'^{17}O$ from their mass-weighted arithmetic mean $\Delta'^{17}O$. The largest deviation occurs when the mass ratio between two water bodies is close to 1:1 (Fig. S3). In terms of magnitude, when two water bodies with a difference of 10‰, 20‰, and 30‰ in $\delta^{18}O$ are mixed, the largest deviation in $\Delta'^{17}O$ at a mass ratio of 1:1 is about 3 per meg, 13 per meg, and 29 per meg, respectively. These magnitudes of deviation are comparable to that of $\Delta(\Delta'^{17}O)$ in our previous Rayleigh distillation analysis. Therefore, there is a need to incorporate mixing effects to investigate the control of precipitation $\Delta'^{17}O$ variability. For example, Li et al. (2015) suggested that the lower precipitation $\Delta'^{17}O$ in the central US is likely a result of vapor mixing among multiple moisture sources.

Here we Introduce a new conceptual model (Fig. 6) that describes the repeated split, distillation, and mixing (RSDM) process of water vapor to understand the mixing effect on precipitation $\Delta'^{17}O$. Given a hypothetical mass of water vapor, we first split it into two aliquots with one undergoing Rayleigh distillation. Next, the remaining vapor is mixed with the other undistilled aliquot. This vapor mixture then iterates through another batch of split, distillation, and mixing repeatedly. In this conceptual model, the key parameter controlling the isotopic evolution of water vapor is the cooling step, i.e., the temperature gradient applied in each batch of Rayleigh distillation. If the temperature gradient is greater resulting in an increased depletion of $\delta^{18}O$ in the remaining vapor, the mixing effect that decreases vapor $\Delta'^{17}O$ is stronger in each batch as mixing occurs between two vapor bodies with a larger contrast in $\delta^{18}O$ (despite mass ratio farther away from 1:1) and will be aggregated after running repeated batches.

To demonstrate the model behavior, we create three RSDM model simulations with cooling steps of 2 °C, 6 °C, and 10 °C when T_d decreases from 25 °C to 0 °C and from 0 °C to −20 °C, again, in order to separate results considering different condensate phases. The d-excess and $\Delta'^{17}O$ of precipitation in each batch of RSDM model simulations are plotted against $\delta^{18}O$ as scatters and are compared to Rayleigh distillation curves in Fig. 7. When condensate is liquid and the largest cooling step of 10 °C is applied, precipitation $\Delta'^{17}O$ has a decreasing trend with the depletion of $\delta^{18}O$. This is in contrast to pure Rayleigh distillation (no mixing) in which precipitation $\Delta'^{17}O$ shows an increasing trend. Ultimately, precipitation $\Delta'^{17}O$ is about 10 per meg lower than in the case of pure Rayleigh distillation (Fig. 7b). However, mixing has little impact on the d-excess between RSDM and Rayleigh model simulations and among different cooling steps (Figs. 7a). When condensate has ice, the mixing

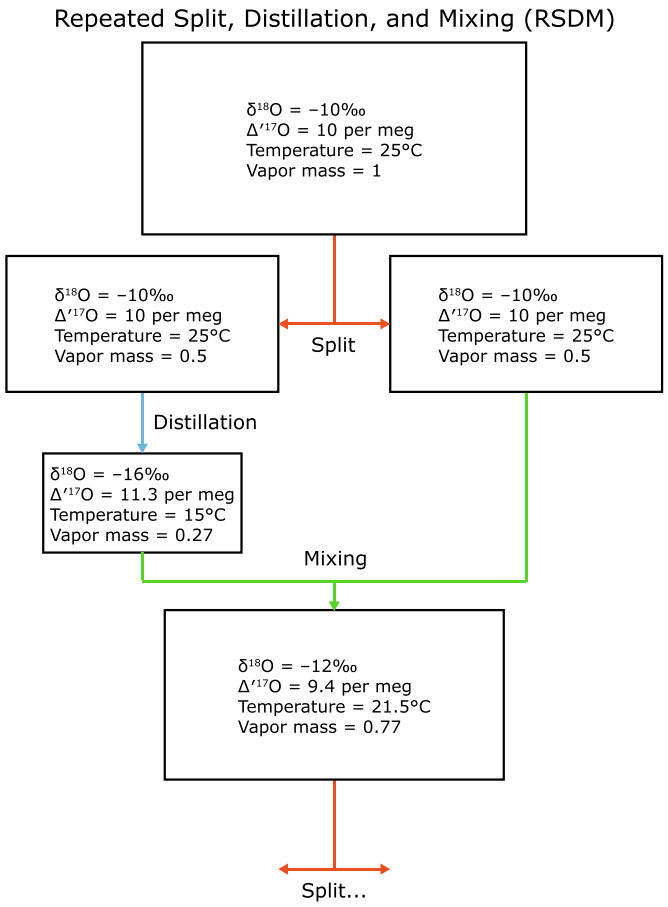

Fig. 6. Schematic of Repeated Split, Distillation, and Mixing (RSDM) model of water vapor.

effect is more conspicuous for $\Delta'^{17}O$; precipitation $\Delta'^{17}O$ is stable at about 25 per meg with cooling steps of 10 °C, but it increases to >50 per meg in the case of pure Rayleigh distillation (Fig. 7d). For d-excess, although mixing does not directly introduce any non-linear behavior, it does flatten the d-excess variation compared to the case of pure Rayleigh distillation with a shift of at most 3‰ (Fig. 7c), a magnitude quite small compared to the strong mixing effect on $\Delta'^{17}O$.

These RSDM model simulations indicate that the interaction between vapor mixing and Rayleigh distillation counteracts the increasing $\Delta'^{17}O$ trend predicted by the Rayleigh distillation model alone but has a smaller effect on d-excess. Although mixing has been already invoked as a potential mechanism to explain the lower precipitation $\Delta'^{17}O$ in observations (Li et al., 2015), the conceptual model developed here aims to show that the same mechanism also operates from the distillation of water vapor derived from a single moisture source and does not require any external source of vapor (to make mixing occur). This mechanism is strongest when i) ice condensation is involved at low T_d, ii) mixing occurs less frequently with larger cooling steps, and iii) there is a high degree of net distillation (low $\delta^{18}O$). It will, in turn, further affect the relationship between d-excess and $\Delta'^{17}O$ in precipitation. However, we acknowledge that we are unable to evaluate how important or how good the RSDM model processes are to represent the reality and we are unaware of any similar models. We therefore caution that the RSDM model developed here is intended for theoretical exploration.

4. Terrestrial moisture recycling and raindrop re-evaporation

In the previous section, we have shown that shifts in precipitation d-excess and $\Delta'^{17}O$ may occur even if the condensation is controlled by liquid-vapor equilibrium fractionation only. In these environments, where the temperature is above the freezing point, however, two additional processes—one remote and one local (Fig. 1a), both comprising a kinetic fractionation component—are known to affect the d-excess and $\Delta'^{17}O$ signals in precipitation (Aron et al., 2021). First, terrestrial evapotranspiration that is ubiquitous over continents recycles precipitated moisture back to the atmosphere and propagates to affect the isotopic composition in downwind water vapor and precipitation (Gat and Matsui, 1991; Gat et al., 1994; Kong et al., 2013; Ampuero et al., 2020). A similar recycling process may also occur when the temperature is below the freezing point by snow sublimation (Fig. 1a) (Kopec et al., 2019; Pang et al., 2019). Second, raindrops are subject to post-condensation evaporation while falling through an unsaturated atmosphere, before local precipitation samples are collected (Stewart, 1975; Liebminger et al., 2006; Wang et al., 2016b; Graf et al., 2019). In this section, we investigate the different sensitivities of d-excess and $\Delta'^{17}O$ in response to these two processes in terms of the magnitude of changes predicted by theoretical models.

4.1. Terrestrial moisture recycling

Terrestrial moisture recycling has been conceptualized as a remote mechanism for increasing d-excess in precipitation. Surface water evaporation from reservoirs such as lakes, soils, and forest canopies, is more complex than evaporation from oceans, but the first-order physics can still be described by the same model by Craig and Gordon (1965), with evaporation fluxes characterized by higher d-excess than surface water supplied to the atmosphere and remaining reservoir conversely left with lower d-excess (Barnes and Allison, 1983; Gat and Matsui, 1991; Gat et al., 1994). The same mechanism also applies to $\Delta'^{17}O$ (Li et al., 2015; Surma et al., 2018; Aron et al., 2021), but there is a lack of knowledge about the different sensitivities between d-excess and $\Delta'^{17}O$ in response to moisture recycling. Recent studies have primarily focused on the characteristics of $\Delta'^{17}O$ in lake water for water balance applications (Surma et al., 2015; Surma et al., 2018; Voigt et al., 2021). For example, Voigt et al. (2021) found that $\Delta'^{17}O$ is more sensitive than d-excess to distinguish the groundwater recharge at steady state and the input of transient runoff. Li et al. (2015) tested two sets of evaporation models and suggested that $\Delta'^{17}O$ and d-excess should vary by 0.7–2 per meg/‰ during progressive evaporation of lake bodies (and similarly in evaporation fluxes). However, open-water evaporation is just one of many evaporation pathways and represents a small fraction of total recycled moisture (Martens et al., 2017). In addition, plant transpiration strongly contributes to moisture recycling; transpiration fluxes on long timescales are seen to retain the same isotopic composition as their source water (Gat and Matsui, 1991; Good et al., 2015; Wang et al., 2016a). Correctly representing the isotopic composition of the total evapotranspiration flux ($^{X}\delta_{ET}$) on different timescales is a major challenge in isotope hydrology as it is controlled by many factors relevant to climate and land surface ecohydrology (Gat and Airey, 2006; Wei and Lee, 2019).

Here we use the same formulation for parameterizing $^{X}\delta_{ET}$ as presented by Xia and Winnick (2021), which enables interactions between evaporation and transpiration fluxes through the closure assumption (Aemisegger et al., 2014), but it is further modified by incorporating simple runoff and water storage terms. This modification is implemented considering that the source water for supplying evapotranspiration fluxes is not only provided by precipitation but also includes surface or subsurface water storage. The new model is intended to represent the mean $^{X}\delta_{ET}$ on seasonal timescales for given particular conditions of water balance, water storage size, and evapotranspiration partitioning. The details are given in Appendix C. In short, we define the amounts of precipitation influx, evapotranspiration outflux, water storage, and runoff outflux as *P*, *ET*, *S*, and *R*, respectively. In the model design, precipitation influx first infiltrates down and is mixed with water storage. Next, a part of this mixture is removed by runoff outflux, which has the same isotopic composition as the mixture. Then, a part of this

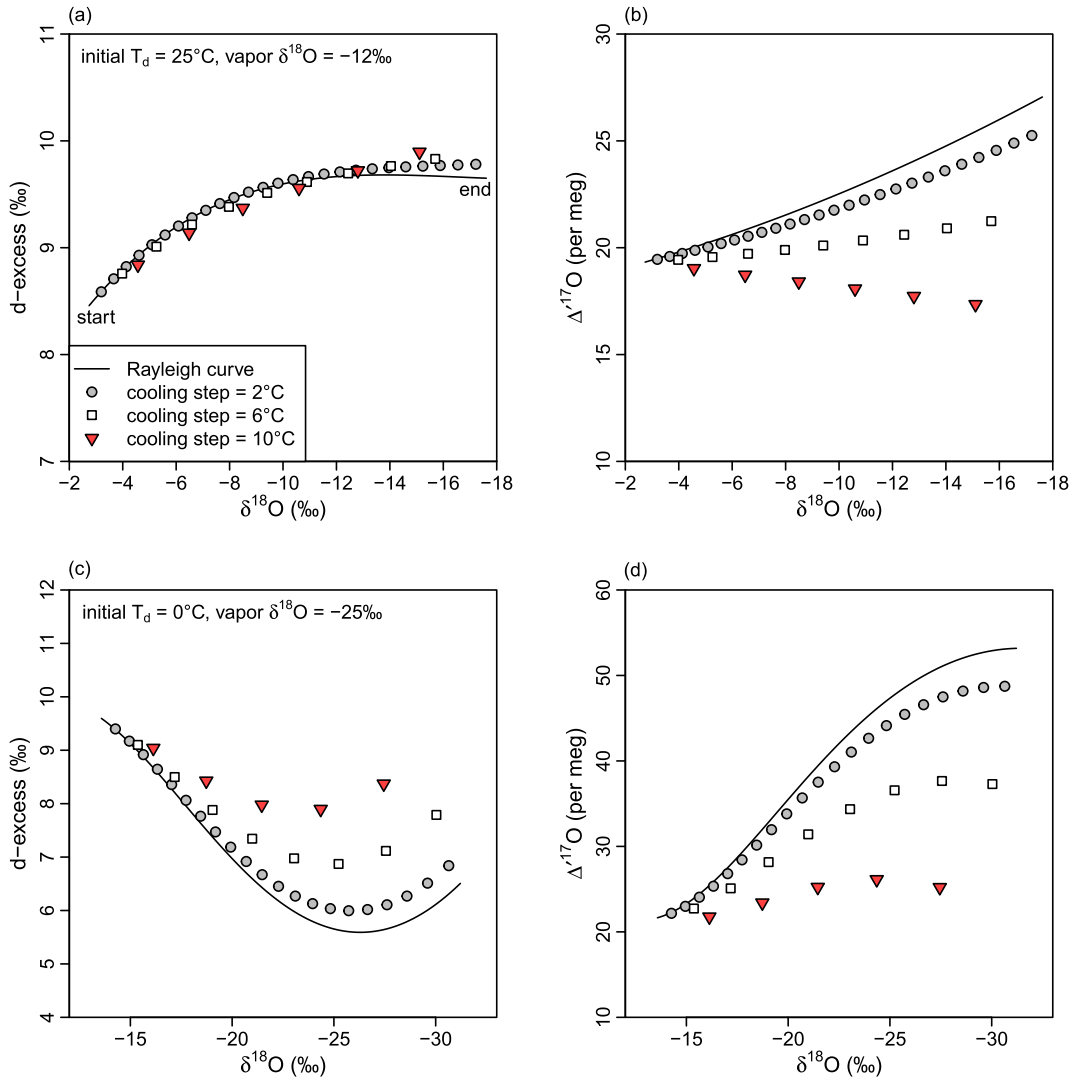

Fig. 7. RSDM model simulations at three different cooling step sizes. Precipitation d-excess (a, c) and $\Delta'^{17}O$ (b, d) versus $\delta^{18}O$ in each iteration are shown as scatters when condensate is liquid (a, b) and when condensate has ice (c, d). Solid black lines are Rayleigh distillation curves (no mixing effect) for comparison. The initial vapor d-excess and $\Delta'^{17}O$ are 10‰ and 10 per meg, respectively. Note that the *x*-axis for $\delta^{18}O$ is inverted.

mixture is further removed by evapotranspiration outflux and is the source water to determine ${}^{X}\delta_{ET}$. At a hydrological steady state, the residual water storage should have the same size as the initial water storage, i.e., $S + P - R - ET = S$, so that $P - R = ET$. At an isotopic steady state, the residual water storage should have the same isotopic composition as the initial water storage, a constraint required to solve ${}^{X}\delta_{ET}$. Our previous work applies a similar water storage framework to derive ${}^{X}\delta_{ET}$ for a pair of wet ($P > ET$) and dry ($P < ET$) seasons (Xia et al., 2022), while we focus on the condition of $P > ET$ at steady state in this study.

We use a simple test of this new model for ${}^{X}\delta_{ET}$ to understand how $\delta^{18}O$, d-excess, and $\Delta'^{17}O$ of evapotranspiration fluxes respond to variations of surface water balances (*ET/P*), relative sizes of water storage (*S/P*), transpiration fractions (*T/ET*), and aerodynamic exponents (*m*), with surface temperature, surface RH, and ${}^{X}\delta_{p}$ kept constant (Figs. 8a–8c). The results indicate that all these factors significantly affect the isotopic composition of evapotranspiration fluxes. Lower *ET/P*, higher *S/P*, lower *T/ET*, and higher *m* values result in lower $\delta^{18}O$, higher d-excess, and higher $\Delta'^{17}O$ of evapotranspiration fluxes. Regarding the relative magnitude of shifts, $\Delta'^{17}O$ is more sensitive than d-excess under higher *ET/P*, lower *S/P*, lower *T/ET*, and higher *m* conditions, as reflected by the higher ratio of their shifts between evapotranspiration and precipitation, i.e., $\Delta(\Delta'^{17}O)/\Delta(\text{d-excess})$ (Fig. 8d). For example, with $ET/P = 0.6$, $S/P = 0.2$, and $m = 0.75$, this ratio is about 2.1 per meg/‰, 1.4 per meg/‰, and 0.5 per meg/‰ when $T/ET = 0.2$, 0.5, and 0.8, respectively, suggesting a different sensitivity by a factor of four (2.1/0.5) to transpiration fractions. When *T/ET* or *ET/P* approaches 1, the d-excess and $\Delta'^{17}O$ of evapotranspiration fluxes approach precipitation values (10‰ and 20 per meg) (Fig. 8b and c). We note that the finding of this variable sensitivity seems unique to our particular model for ${}^{X}\delta_{ET}$. The same analysis of ${}^{X}\delta_{ET}$ in three sub-models presented by Gat and Matsui (1991), which have different parameterizations from ours (no closure assumption is the major distinction), shows that the $\Delta(\Delta'^{17}O)/\Delta(\text{d-excess})$ is between 2 and 2.5, regardless the values of different parameters (Fig. S4).

Next, we test whether the different sensitivities of d-excess and $\Delta'^{17}O$ of evapotranspiration fluxes are fully propagated through moisture recycling to affect downwind water vapor and precipitation. A complication here is that moisture recycling essentially is a mixing process for which it is known that non-linearity will be introduced for $\Delta'^{17}O$ (Section 3.2). For this purpose, the Rayleigh distillation model is coupled with moisture recycling and becomes a reactive transport model in which atmospheric water vapor is transported through advection and exchanges with the land surface through precipitation and evapotranspiration fluxes (Winnick et al., 2014). The details are given in Appendix

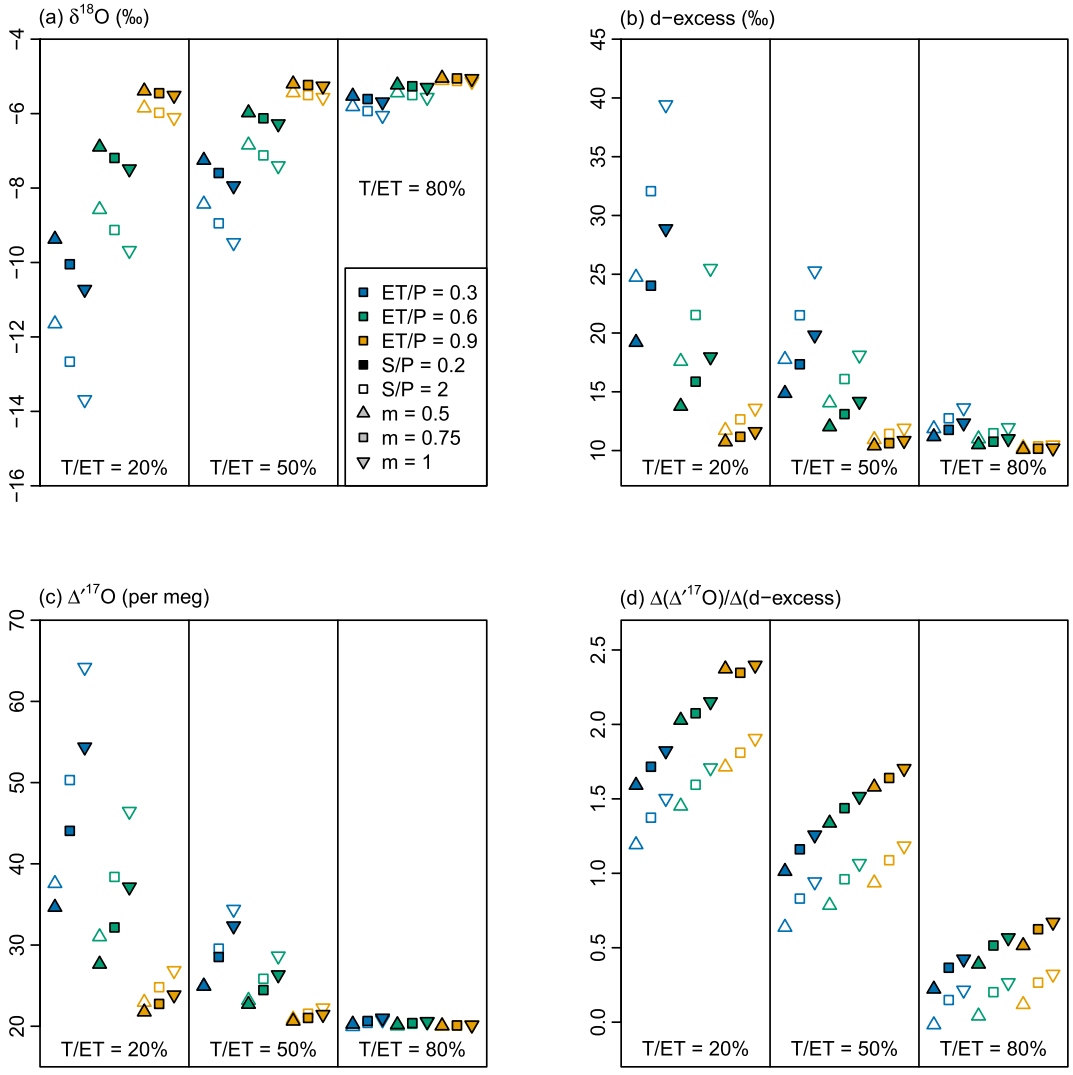

Fig. 8. The new model for the isotopic composition of evapotranspiration fluxes (δ_{ET}). The $\delta^{18}O$ (a), d-excess (b), and $\Delta'^{17}O$ (c), as well as the $\Delta(\Delta'^{17}O)/\Delta$(d-excess) (d) of evapotranspiration fluxes relative to precipitation inputs. Each parameter is calculated for three water balance ratios (*ET/P*, indicated by color), two water storage ratios (*S/P*, indicated by either open or closed symbol), three transpiration fractions (*T/ET*, horizontally separated in three fields), and three aerodynamic exponents (*m*, indicated by symbol shape), under the following model inputs: surface temperature = 22 °C, surface RH = 70%, precipitation $\delta^{18}O = -5$‰, d-excess = 10‰, and $\Delta'^{17}O = 20$ per meg.

D. Fig. 9 shows that the different sensitives of d-excess and $\Delta'^{17}O$ of evapotranspiration fluxes are indeed propagated downwind and mainly controlled by transpiration fractions and, to a lesser extent, other factors (Fig. 9). For example, when $T/ET = 20\%$, precipitation d-excess and $\Delta'^{17}O$ at the end of profiles are not only both increased in a larger degree relative to the case of Rayleigh distillation but also are characterized by a higher ratio of shifts, $\Delta(\Delta'^{17}O)/\Delta$(d-excess), up to about 3 per meg/‰ (Fig. 9c and d). When $T/ET = 80\%$, precipitation d-excess and $\Delta'^{17}O$ at the end of profiles change very little with low $\Delta(\Delta'^{17}O)/\Delta$(d-excess) at about 1 per meg/‰.

Overall, we use these theoretical approximations to demonstrate that the d-excess and $\Delta'^{17}O$ of precipitation have a common response to upwind moisture recycling with a different sensitivity. This suggests the potential use of paired precipitation d-excess and $\Delta'^{17}O$ data to constrain the recycling mechanism such as the partitioning of evapotranspiration fluxes. However, this idea is based on the analysis carried out with our particular ${}^{X}\delta_{ET}$ model and under the assumption $P > ET$. The broad applicability of paired measurements in environments that fall outside these constraints requires further evaluation. Our previous work highlights that the $P < ET$ condition (like large lake basins) is widespread seasonally on continents, which become a net moisture source rather than sink (Xia et al., 2022), while we lack a simple parameterization for ${}^{X}\delta_{ET}$ under this condition. Therefore, there might be a more complex relationship between d-excess and $\Delta'^{17}O$ induced by terrestrial moisture recycling not reflected in our analysis.

4.2. Raindrop re-evaporation

Raindrop re-evaporation has been frequently invoked to explain the low d-excess in local precipitation observed in arid regions or during dry periods (Gat, 1996; Liebminger et al., 2006; Pang et al., 2011; Putman et al., 2019), and again, should similarly affect $\Delta'^{17}O$ (Aron et al., 2021). In terms of the isotopic fractionation mechanism, evaporation from raindrops is analogous to evaporation from oceans and lakes; kinetic fractionation occurs in the diffusional transport of water vapor from the raindrop-air interface to the ambient atmosphere, despite the fact that evaporation rates are roughly an order of magnitude higher for raindrops (Stewart, 1975). The isotopic evolution of falling raindrops is also affected by the isotopic composition of sub-cloud water vapor which is highly variable within and among precipitation events (Bony et al., 2008; Risi et al., 2008; Kurita, 2013; Graf et al., 2019). If the sub-cloud atmosphere is saturated, raindrops gradually evolve to attain the

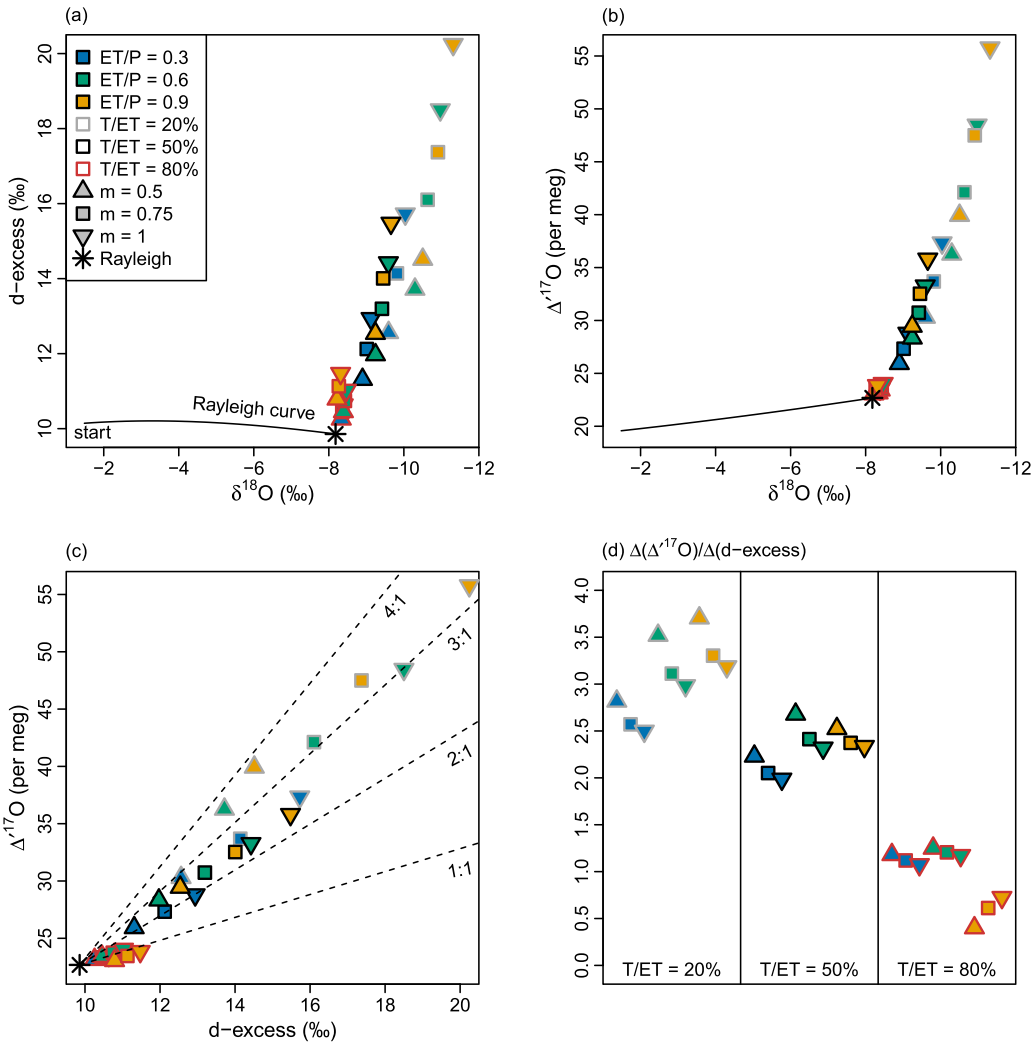

Fig. 9. The effect of terrestrial moisture recycling in the reactive transport model of water vapor. The isotopic compositions of precipitation at the end of profiles are shown as scatters between (a) d-excess and $\delta^{18}O$, (b) $\Delta'^{17}O$ and $\delta^{18}O$, and (c) $\Delta'^{17}O$ and d-excess, when models are run at three water balance ratios (*ET/P*, indicated by color) three transpiration fractions (*T/ET*, horizontally separated in three fields), and three aerodynamic exponents (*m*, indicated by symbol shape). The results from the Rayleigh distillation model that has no moisture recycling component is shown for comparison (asterisks). In (a) and (b), note that the *x*-axis for $\delta^{18}O$ is inverted. In (c), different slopes between $\Delta'^{17}O$ and d-excess shifts relative to the case of Rayleigh distillation are plotted as black dashed lines for reference. The ratios of shifts in $\Delta'^{17}O$ and d-excess in reactive transport models relative to the case of Rayleigh distillation, $\Delta(\Delta'^{17}O)/\Delta$(d-excess), are plotted in (d). The initial isotopic composition of water vapor is: $\delta^{18}O = -11‰$, d-excess = 10‰, and $\Delta'^{17}O = 10$ per meg. The initial T_d is 22 °C and final T_d is 10 °C. The surface RH is constant at 70% across the profile. The surface temperature across the profile is calculated from the Clausius–Clapeyron relation (Bolton, 1980). The water storage size *S/P* is 0.2 across the profile.

isotopic equilibrium with ambient water vapor without re-evaporation, a process referred to as equilibration (Stewart, 1975; Lee and Fung, 2008). If the sub-cloud atmosphere is unsaturated, re-evaporation fluxes of raindrops dominate and compete against their tendency towards equilibration. Since the raindrop-vapor interaction and related isotopic exchange are complex, simple idealized models are useful to characterize the response and sensitivity of d-excess and $\Delta'^{17}O$ to raindrop re-evaporation.

Stewart (1975) investigated the isotopic fractionation in raindrop re-evaporation with laboratory experiments and presented an isotopic model that has been widely adopted (Appendix E). However, the formulation of that model is for simulating the isotopic composition of a raindrop at a constant ambient condition and a prescribed amount of evaporation (Fig. S5), and thus does not necessarily represent dynamic processes when raindrops are falling through the air with changing ambient conditions with height.

Instead, we focus on the dynamic raindrop re-evaporation model that uses heat and mass transfer equations to simulate changes in temperature, mass, and isotopic ratio of the raindrop falling through an unsaturated air column numerically until it hits the ground (Graf et al., 2019). The model codes are available in Xia and Winnick (2021). The model inputs are surface temperature and surface RH, which determine the lifting condensation level (LCL) and vertical profiles of temperature and RH, along with raindrop diameter. Two important assumptions are made. First, the raindrop is formed and released to fall at the height of LCL, and second, the initial raindrop is in isotopic equilibrium with the homogeneous sub-cloud water vapor (Xia and Winnick, 2021). To test the model behavior, this dynamic model is run over a range of surface temperature and surface RH for three initial raindrop diameters of 0.8 mm, 1.6 mm, and 2.4 mm that correspond to light, intermediate, and heavy rainfall events, respectively. The results shown in Fig. 10 suggest that a lower surface RH (by increasing the height of LCL) or a smaller raindrop size (by decreasing the falling velocity of the raindrop) results in a larger decrease of d-excess and $\Delta'^{17}O$ as well as a higher $\Delta(\Delta'^{17}O)/\Delta$(d-excess) in raindrops. The smaller raindrop size seems more critical than the lower surface RH in producing the higher $\Delta(\Delta'^{17}O)/\Delta$(d-excess). For example, at the surface temperature of 20 °C, the following two conditions of surface RH and raindrop diameter have the same 10‰ d-excess decrease: i) 71% and 0.8 mm; ii) 47% and 2.4 mm (Fig. 10b). However, these two conditions have a ratio of 1.71 per meg/‰ and 0.94 per meg/‰ for $\Delta(\Delta'^{17}O)/\Delta$(d-excess), respectively (Fig. 10d). Additionally, in our model output, the $\Delta(\Delta'^{17}O)/\Delta$(d-excess) varies from <0.7 per meg/‰ to >2.5 per meg/‰ (Fig. 10d). By contrast, Landais et al. (2010) tested the other parameterization of raindrop re-evaporation employed in an isotope-enabled GCM and suggested that precipitation $\Delta'^{17}O$ and d-excess should vary by 1.6–2 per meg/‰. Therefore, our model output indicates a possibly wider range of $\Delta(\Delta'^{17}O)/\Delta$(d-excess) in response to the raindrop re-evaporation effect.

Our simple model analysis indicates that the d-excess and $\Delta'^{17}O$ of precipitation also have a common response but with a different sensitivity to local raindrop re-evaporation. Theoretically, this $\Delta(\Delta'^{17}O)/\Delta$(d-excess) may distinguish the controls of surface climate conditions

(surface RH) and rainfall rate (distribution of raindrop sizes) on the re-evaporation effect. However, this idea is based on the results of a highly idealized scenario of raindrop re-evaporation that does not fully account for the complex reality encountered in rainfall events. For example, raindrops may be formed at a higher, freezing level above the LCL and the isotopic composition of sub-cloud water vapor might not be in equilibrium with the initial raindrop, leading to additional isotopic exchange associated with the tendency towards equilibration (Graf et al., 2019). Therefore, the relationship between d-excess and $\Delta'^{17}O$ in sub-cloud processes is also likely much more complex than what we have shown. It demands coupled isotopic measurements of water vapor and precipitation for disentangling these complex mechanisms in the future (Surma et al., 2021).

5. Data-model comparison

The above sections have interrogated the major hydroclimate processes that affect d-excess and $\Delta'^{17}O$ in precipitation based on theoretical models, with an emphasis on their common and distinct features. In this section, we examine the overall pattern in precipitation $\delta^{18}O$, d-excess, and $\Delta'^{17}O$ variations that have emerged from observational data and develop a stochastic simulation approach to understand whether and how theoretical models correctly reproduce the observed patterns.

5.1. Isotope data

We have compiled all triple oxygen isotope data from measurements of precipitation including polar snow currently available in the literature (Tables S1 and S2). These data are measured from samples with temporal resolutions from event to monthly-integrated precipitation or even longer for polar snow (that may represent multiple years of accumulation). This database also contains paired d-excess data that are reported in original studies. To assist in our analysis, the Global Network of Isotopes in Precipitation (GNIP) database that contains a large amount of monthly d-excess measurements is also examined (IAEA/WMO, 2022). Individual data that meet the following criteria are included: $-25‰ < \delta^{18}O < 5‰$, $-20‰ <$ d-excess $<40‰$, and -40 per meg $< \Delta'^{17}O < 80$ per meg. We exclude those data with extremely low $\delta^{18}O$ values ($< -25‰$) commonly found over ice sheets, since in these very cold regions, precipitation d-excess and $\Delta'^{17}O$ become highly

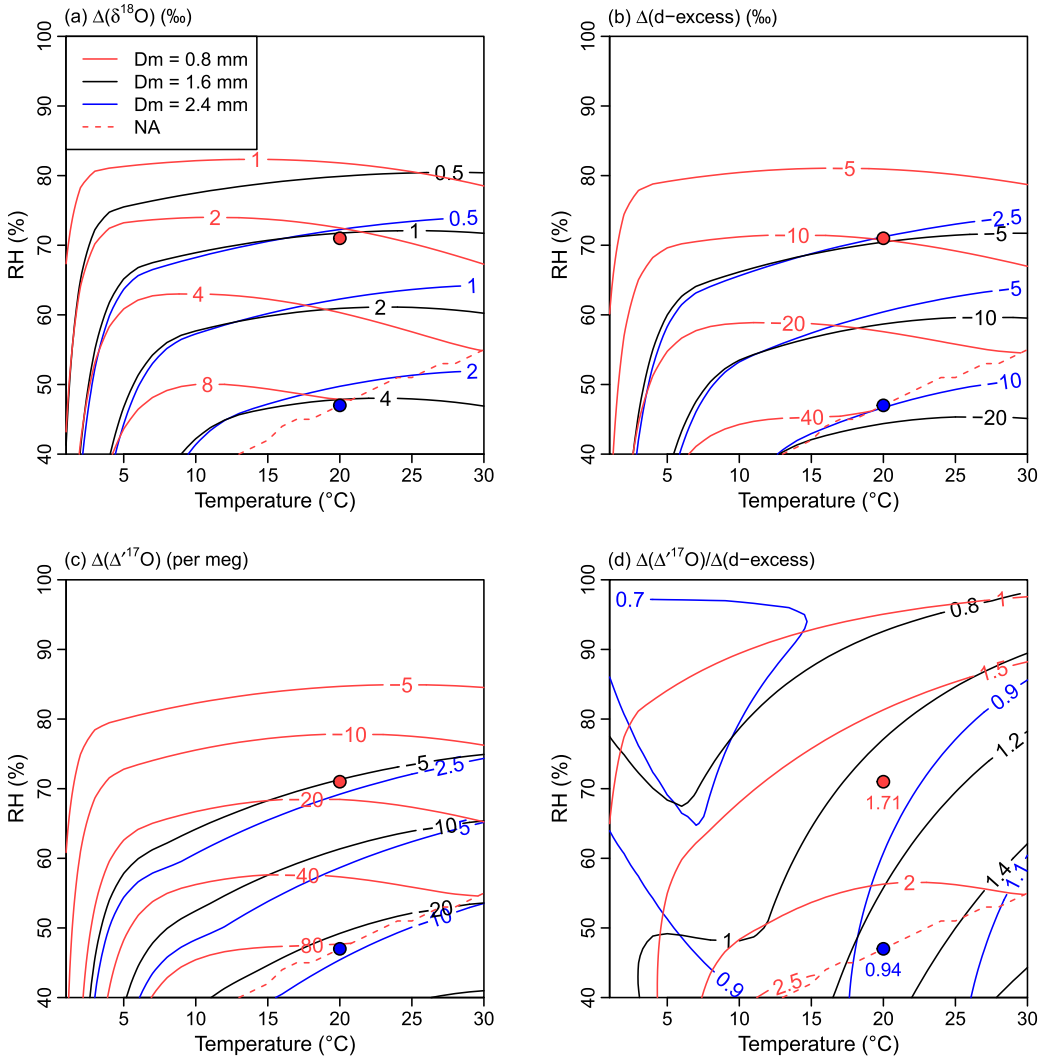

Fig. 10. The effect of raindrop re-evaporation. Shifts in isotopic compositions of raindrops relative to initial values under different surface temperature and surface RH are shown as contour lines at three initial raindrop diameters (*Dm*, indicated by color) for (a) $\Delta(\delta^{18}O)$; (b) Δ(d-excess); (c) $\Delta(\Delta'^{17}O)$; and (d) $\Delta(\Delta'^{17}O)/\Delta$(d-excess). The initial isotopic composition of the raindrop is: $\delta^{18}O = -8‰$, d-excess = 10‰, $\Delta'^{17}O = 20$ per meg. Two scatter points indicate two conditions that produce the same Δ(d-excess) but with a very different $\Delta(\Delta'^{17}O)/\Delta$(d-excess) (see main text). Note that when the initial raindrop diameter is 0.8 mm, the raindrop will be completely evaporated at high surface temperature and low surface RH conditions (indicated by dashed lines).

sensitive to the elusive cloud microphysics, snow formation mechanism, and snow sublimation cycle (Miller, 2018; Dütsch et al., 2019; Pang et al., 2019). We intentionally narrow the scope of our analysis to the d-excess and $\Delta'^{17}O$ variability that characterizes low- and mid-latitude regions. We also speculate that those uncommon data with very low or high d-excess and $\Delta'^{17}O$ have a greater likelihood to be measurement errors (Xia et al., 2022). While studies that reported triple oxygen isotope data have provided their own analyses and interpretations, we here focus on two key patterns of these data as a whole. First, we investigate the trends of d-excess and $\Delta'^{17}O$ versus $\delta^{18}O$ to understand how these two parameters vary in response to large-scale distillation gradients encapsulated in precipitation $\delta^{18}O$. Second, we evaluate the overall relationship between available paired d-excess and $\Delta'^{17}O$ data to understand the commonality and distinction between these two parameters.

The GNIP-based d-excess data are shown in Fig. 11a as the mean and 2σ standard deviation at each 1‰ bin of $\delta^{18}O$. Precipitation d-excess is stable at 10‰ for $\delta^{18}O < 0$‰ and becomes lower as $\delta^{18}O$ increases above 0‰. The 2σ standard deviation of d-excess is about ±12‰ for $\delta^{18}O <$ 0‰ and is as high as ±18‰ for $\delta^{18}O > 0$‰. The compiled literature-based $\Delta'^{17}O$ and d-excess data are plotted in Fig. 11b and c along with the mean and 2σ standard deviation at each 5‰ bin of $\delta^{18}O$. For $\Delta'^{17}O$, the binned mean value increases steadily from 20 per meg to 35 per meg as $\delta^{18}O$ decreases from 0‰ to −25‰ and is very low at about −5 per meg when $\delta^{18}O$ exceeds >0‰. The 2σ standard deviation is roughly about ±30 per meg. The d-excess data from the compiled $\Delta'^{17}O$ database follow a similar trend to GNIP-based d-excess data, except that the 2σ standard deviation of d-excess from the compiled literature database is smaller for $\delta^{18}O < -20$‰. This comparison of d-excess data between the GNIP database and our compiled literature database provides a validation that the currently available $\Delta'^{17}O$ data are sufficiently representative for the analysis of their overall pattern. However, we speculate that precipitation $\Delta'^{17}O$ data with $\delta^{18}O$ ranging from −25‰ to −20‰ are currently underrepresented in the literature, and thus, we may also have underestimated the degree of variability in $\Delta'^{17}O$ at low $\delta^{18}O$. Finally, the scatter plot between $\Delta'^{17}O$ and d-excess is shown in Fig. 11d. These data appear to have a very weak but statistically significant positive correlation ($R^2 = 0.07$, $p = 10^{-16}$, $n = 1427$), and the orthogonal distance regression line has the equation: $\Delta'^{17}O$ (per meg) = 8.3(±0.6) × d-excess (‰) – 52.6(±5.8).

In summary, two key patterns emerge from observational data. First, despite the large variability, the mean precipitation d-excess does not

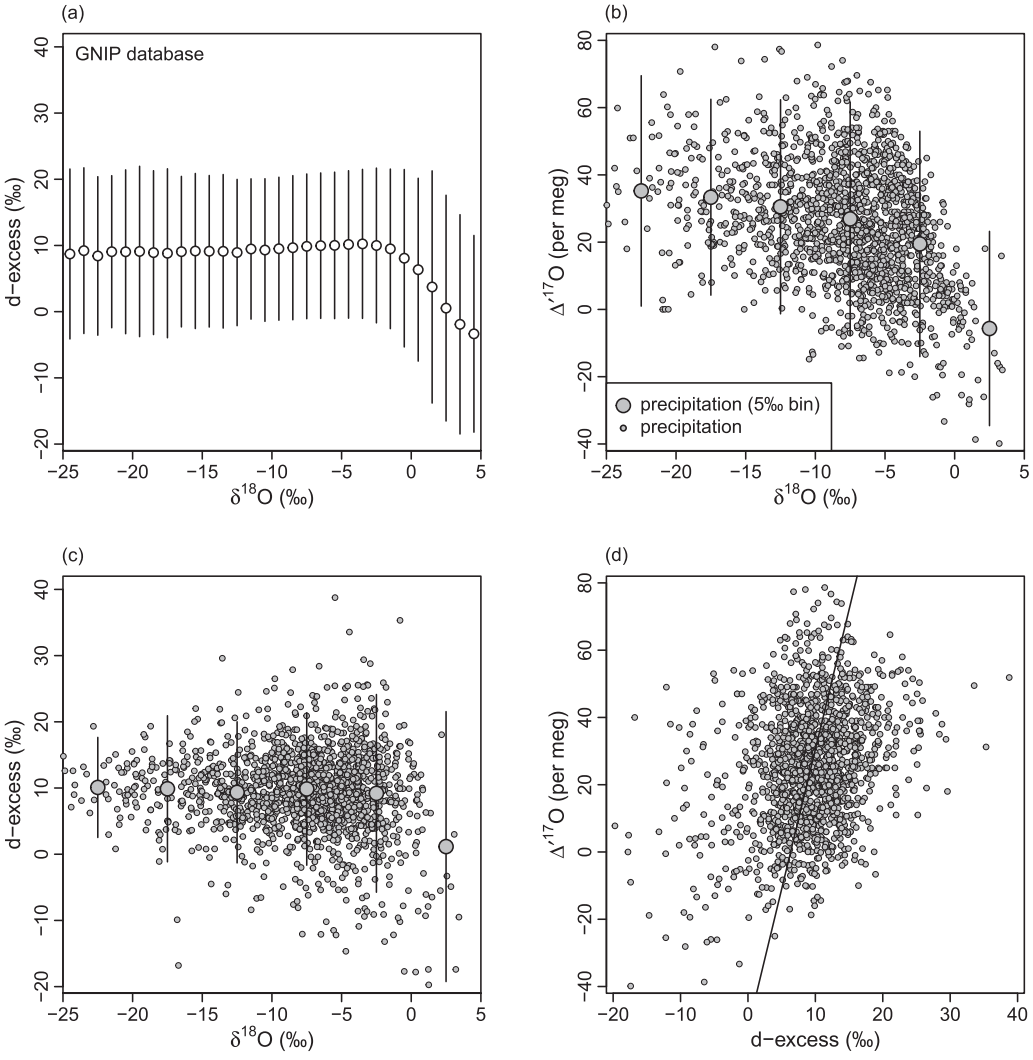

Fig. 11. The pattern of precipitation d-excess and $\Delta'^{17}O$ data in observations. (a) The mean and 2σ standard deviation of d-excess at each 1‰ bin of $\delta^{18}O$ from GNIP database. (b) The scatter between $\Delta'^{17}O$ and $\delta^{18}O$ data in compiled triple oxygen isotope database for precipitation. Large dots and error bars are the mean and 2σ standard deviation of $\Delta'^{17}O$ at each 5‰ bin of $\delta^{18}O$. (c) Similar to (b), but for d-excess and $\delta^{18}O$ data in compiled triple oxygen isotope database if paired d-excess data are available. (d) The scatter between paired $\Delta'^{17}O$ and d-excess data. The solid line is the orthogonal distance regression line.

vary with $\delta^{18}O$, and the mean precipitation $\Delta'^{17}O$ increases by 15 per meg following the distillation gradient of decreasing $\delta^{18}O$. Additionally, both precipitation d-excess and $\Delta'^{17}O$ become much lower in the range of positive $\delta^{18}O$ values. Second, for paired precipitation d-excess and $\Delta'^{17}O$ data, their correlation is very weak and their regression coefficient implies that $\Delta'^{17}O$ is much more variable than d-excess by a factor of >8 (per meg/‰).

5.2. Model simulations

In this subsection, we investigate whether and how current theoretical models of isotopic fractionation are capable to capture the above two key patterns in the overall relationship among $\delta^{18}O$, d-excess, and $\Delta'^{17}O$ in precipitation. The aim is to use this simple data-model comparison to evaluate and understand the capabilities and limitations of isotopic models we have examined in previous sections.

To this aim, we develop a stochastic simulation framework to create a model-based dataset of pseudo-precipitation $\delta^{18}O$, d-excess, and $\Delta'^{17}O$. The model inputs and sampling procedures are described in detail in Appendix F. In brief, we run numerous ($n = 10^6$) simulations of the Rayleigh distillation-based forward model, which can be made more complex by incorporating additional processes. In each simulation, the initial and final conditions that control the simulation are sampled from the probability distribution of parameters represented in reanalysis products and GCM outputs, and the simulated isotopic composition of pseudo-precipitation at the end of the distillation profile is collected. The isotopic patterns that emerge from this synthetic dataset are analyzed in comparison with observational data. This approach differs from previous polar snow-based studies that rely on tuning model parameters to proper values in order to fit the general trends of d-excess and $\Delta'^{17}O$ versus $\delta^{18}O$ in observations (Landais et al., 2008; Winkler et al., 2012; Pang et al., 2015). In our approach, the data-model comparison is treated as a statistical problem and used to identify model deficiencies rather than to tune model parameters. We assume that any evaporation flux over oceans is likely the moisture source for any precipitation flux over continents if there is a thermodynamic gradient of decreasing T_d established from source to sink regardless of whether it is dynamically possible. For example, if the moisture source is sampled from the warm tropical ocean with T_d of 25 °C and the moisture sink is sampled from the high-latitude inland area with T_d of −5 °C, a Rayleigh distillation simulation is established across the T_d gradient to derive the isotopic composition of pseudo-precipitation at the end of the distillation profile without considering the dynamics of atmospheric circulation.

We use a series of such simulations stepwise to interrogate the hydroclimate processes that are necessary to achieve the data-model fit. These simulations are introduced briefly here for an overview. In stochastic simulation #1, the simulation is based on the Rayleigh distillation model only. In stochastic simulation #2, the simple raindrop re-evaporation effect is incorporated into simulation #1. In stochastic simulation #3, the vapor mixing effect is incorporated into simulation #2. In stochastic simulation #4, an equilibration component is applied to the raindrop re-evaporation model built upon simulation #3. In stochastic simulation #5, a larger perturbation of $\Delta'^{17}O$ due to the analytical error is added into simulation #4. In stochastic simulation #6, a delayed transition into ice-vapor fractionation is added into simulation #1.

The results of stochastic simulation #1, which again is based on the Rayleigh distillation model only, are shown in Fig. 12a as the mean and 2σ standard deviation of d-excess and $\Delta'^{17}O$ at each 1‰ bin of $\delta^{18}O$, as well as in a frequency plot with the orthogonal distance regression line between $\Delta'^{17}O$ and d-excess. In this synthetic dataset, there are no data with $\delta^{18}O > 0$‰ because the raindrop re-evaporation effect is not incorporated and the highest possible oceanic vapor $\delta^{18}O$ is −10‰ in the sampled GCM (Appendix F). The simulation results reproduce the trends of d-excess and $\Delta'^{17}O$ versus $\delta^{18}O$ reasonably well for $\delta^{18}O > -20$‰, but d-excess and $\Delta'^{17}O$ values become relatively lower and higher, respectively, compared to observational data for $\delta^{18}O < -20$‰. The $\Delta'^{17}O$ and d-excess are clearly decoupled and their regression line is almost vertical due to the incorrectly simulated low d-excess and high $\Delta'^{17}O$ values at low $\delta^{18}O$ (Fig. 12a). The ability of Rayleigh distillation model to reproduce the increasing trend of $\Delta'^{17}O$ versus decreasing $\delta^{18}O$ is an interesting finding that differs from the view that $\Delta'^{17}O$ should be conserved (Aron et al., 2021; Aron et al., 2023); this relates to our treatment that requires decreasing T_d to force the distillation and that supersaturation is involved once $T_d < 0$ °C.

In stochastic simulation #2, the simple raindrop re-evaporation effect is incorporated (Appendix F). With this modification, the low d-excess and $\Delta'^{17}O$ values for $\delta^{18}O > 0$‰ are reproduced, but the model output values are too low compared to observational data. In addition, compared to stochastic simulation #1, the raindrop re-evaporation effect not only decreases d-excess and $\Delta'^{17}O$ at high $\delta^{18}O$ but also further increases them at low $\delta^{18}O$ (Fig. 12b). These relative increases of d-excess and $\Delta'^{17}O$ at low $\delta^{18}O$ reflect the downwind impacts of raindrop re-evaporation through recycling (Li and Garzione, 2017; Xia and Winnick, 2021)—the re-evaporation flux that locally lowers the d-excess and $\Delta'^{17}O$ in precipitation in turn progressively increases them in downwind water vapor and precipitation (see Fig. 1). The overall misfit between data and stochastic simulation #2, in particular, the simulated higher precipitation $\Delta'^{17}O$ values up to 60 per meg at low $\delta^{18}O$ (Fig. 12b), suggests that other processes need to be incorporated for a data-model fit.

In stochastic simulation #3, the vapor mixing effect based on the RSDM model is incorporated. After several trials, we find that mixing by a cooling step of 6 °C, when coupled to each distillation profile, effectively prevents the sharp increase of $\Delta'^{17}O$ for $\delta^{18}O < -20$‰ and results in a better data-model fit (Fig. 12c).

Still, an additional mechanism is required to counteract the raindrop re-evaporation effect that simulates the lower d-excess and $\Delta'^{17}O$ for $\delta^{18}O > 0$‰ compared to observational data (Fig. 12c). As discussed in Section 4.1, terrestrial moisture recycling may strongly impact precipitation d-excess and $\Delta'^{17}O$. However, it is challenging to incorporate this effect into the simulation as there are multiple model parameters involved and their probability distributions and inter-relationships are not well characterized. For example, *ET/P*, *T/ET*, and *S/P* are not independent parameters and each may vary with others, but few studies have explicitly characterized these ecohydrological interactions (Maxwell and Condon, 2016; Xia et al., 2022). Also, as discussed later in Section 5.3, there is a major limitation in our δ_{ET} model that is developed only for $P > ET$ conditions. These together lead us to consider other possible solutions. In stochastic simulation #4, we test adding an equilibration component to the raindrop re-evaporation model for reducing the magnitude of decrease in precipitation d-excess and $\Delta'^{17}O$ at high $\delta^{18}O$. This is accomplished by setting the sub-cloud water vapor in the model to slightly higher d-excess and $\Delta'^{17}O$ values than that in equilibrium with the initial raindrop (see Xia and Winnick, 2021). After several trials, we find that simulation results after setting the sub-cloud water vapor d-excess 3‰ higher and $\Delta'^{17}O$ 4 per meg higher best reproduce the overall trends for both d-excess and $\Delta'^{17}O$ in the full range of $\delta^{18}O$ from −25‰ to 5‰ (Fig. 13a). This modification, although arbitrary, can be thought of to represent the realistic feedback that continuous re-evaporation fluxes of raindrops are likely to increase the d-excess and $\Delta'^{17}O$ of sub-cloud water vapor gradually as rainfall events proceed, bringing in equilibration behavior. This data-model fit suggests that raindrop re-evaporation does not decrease precipitation d-excess and $\Delta'^{17}O$ as strongly as predicted by stochastic simulation #2 in which the initial raindrop is set to be in equilibrium with the sub-cloud water vapor (Liebminger et al., 2006; Froehlich et al., 2008; Xia and Winnick, 2021). Rather, the results indicate that the tendency towards equilibration with sub-cloud water vapor is likely universal and acts to reduce the magnitude of these decreases.

Notably, in stochastic simulation #4, there are still two features not

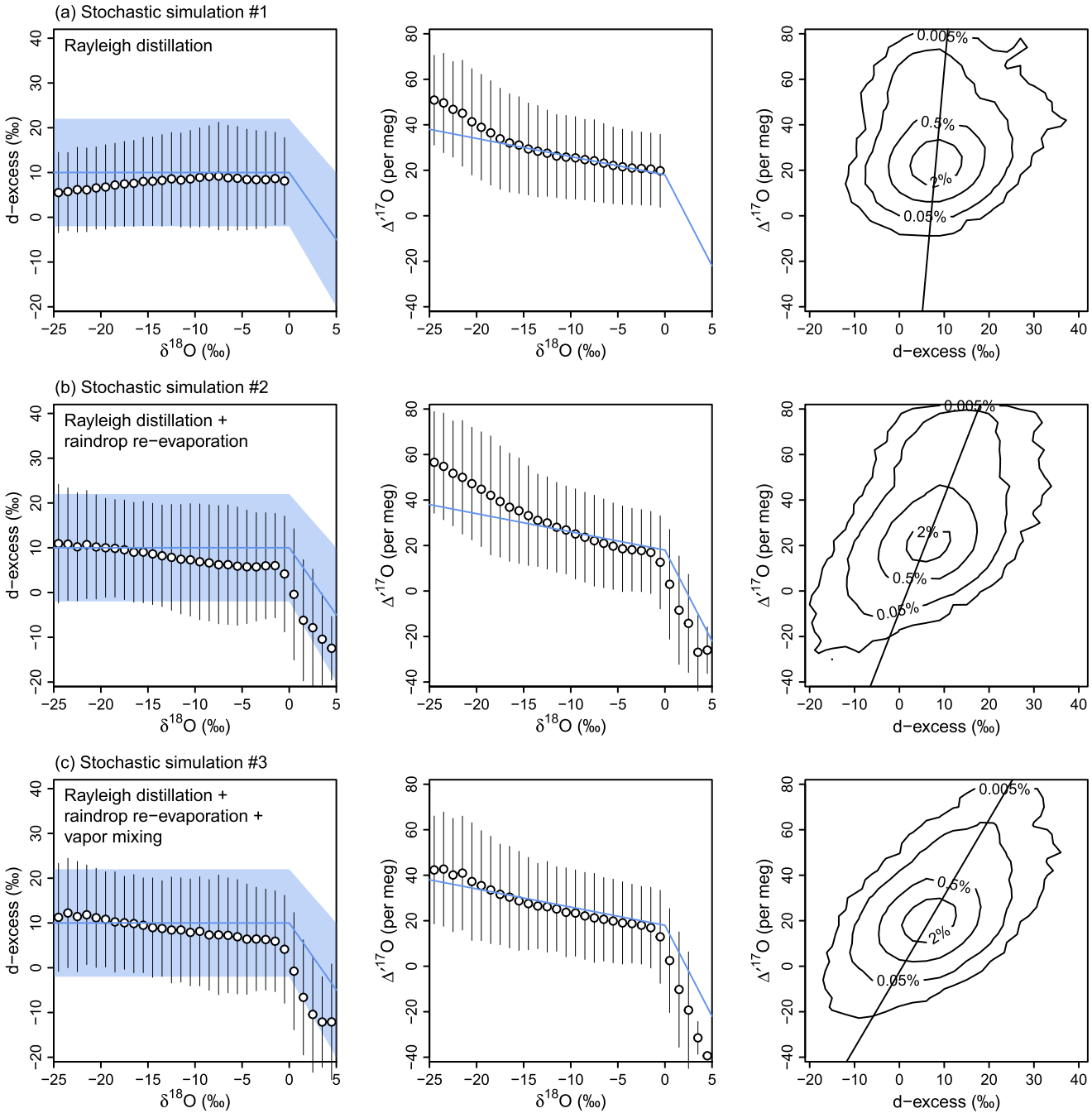

Fig. 12. Results of stochastic simulations #1, #2, #3, shown as the mean and 2σ standard deviation of d-excess and $\Delta'^{17}O$ at each 1‰ bin of $\delta^{18}O$, as well as the frequency plot with orthogonal distance regression line between $\Delta'^{17}O$ and d-excess. The blue lines indicate the general trends of d-excess (the light blue area denotes the range of 2σ standard deviation) and $\Delta'^{17}O$ versus $\delta^{18}O$ from observational data for comparison (see Fig. 11). (For interpretation of the references to color in this figure legend, the reader is referred to the web version of this article.)

correctly represented: the 2σ standard deviation of $\Delta'^{17}O$ in simulations is smaller than in observations, and therefore the regression coefficient between $\Delta'^{17}O$ and d-excess is lower (less steep) than 8 (Fig. 13a). What could be the cause for the wide range of variability in precipitation $\Delta'^{17}O$ in observations? The fact that previous simulations have correctly represented the range of variability in d-excess leads us to hypothesize that numerical values of $\Delta'^{17}O$ data currently available in the literature might contain large analytical errors. As described in Appendix F, in our simulations we have added a small perturbation of ±5 per meg (1σ) for each pseudo-precipitation $\Delta'^{17}O$ to stand for the least level of analytical error (Luz and Barkan, 2010). However, the recent comprehensive review by Aron et al. (2021) gives an estimate of the current analytical error for $\Delta'^{17}O$ at about ±10 per meg. Another inter-laboratory performance study suggests that $\Delta'^{17}O$ data measured from laser spectrometry often overstate the achieved level of precision due to inappropriate methodological protocols (Wassenaar et al., 2021). Enlightened by these findings, in stochastic simulation #5, we test an increased level of $\Delta'^{17}O$ perturbation at ±10 per meg. New simulation results reproduce the relationship between $\Delta'^{17}O$ and d-excess more closely with a higher regression coefficient at about 7.3 ± 0.1 (Fig. 13b), suggesting that the large analytical error in $\Delta'^{17}O$ might be the cause for the steep regression line in observations.

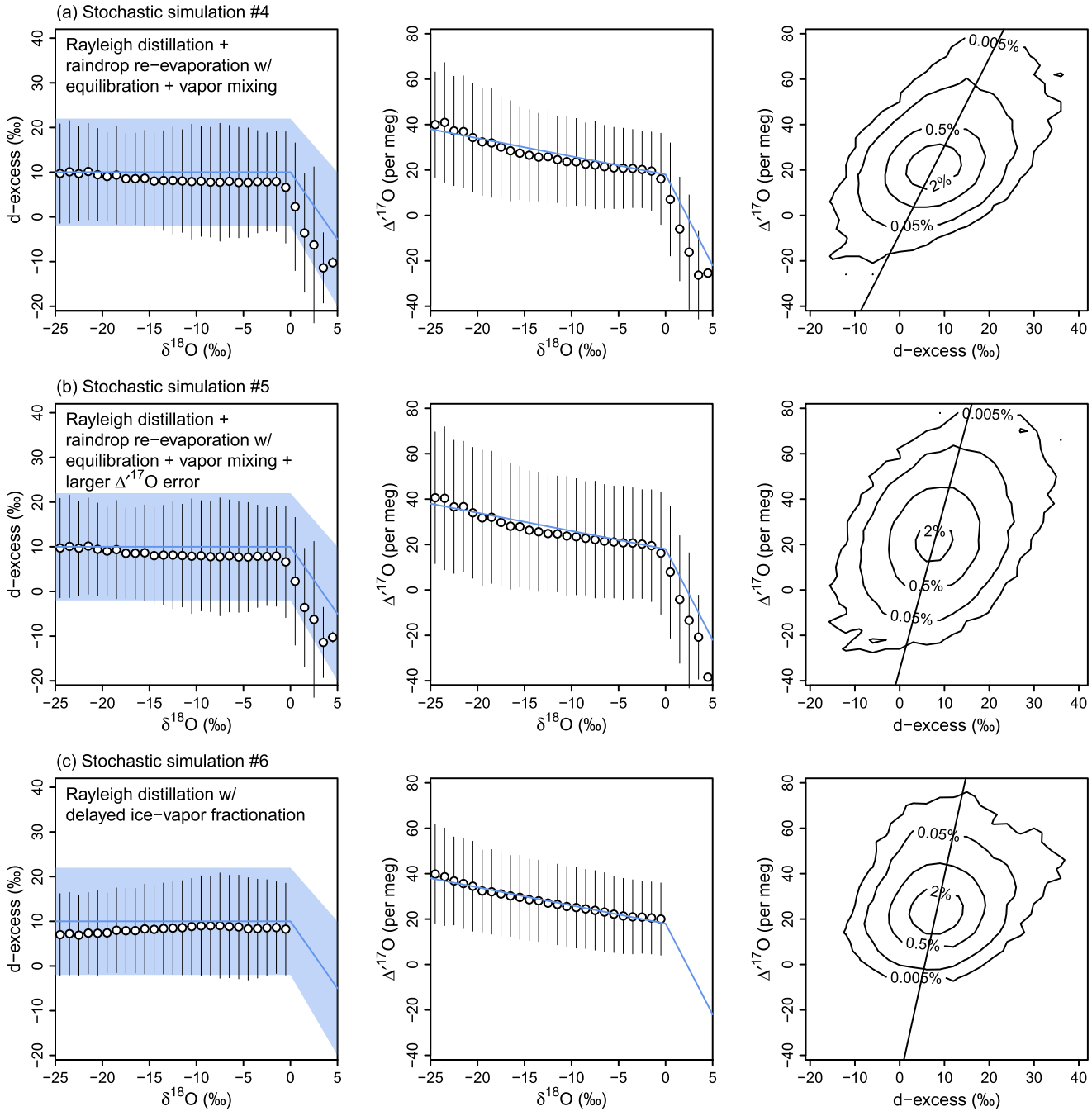

Fig. 13. Same as Fig. 12 but for stochastic simulations #4, #5 and #6.

Finally, we emphasize that the above efforts to reach a data-model fit have not yet considered the accuracy in the parameterization of ice-vapor fractionation, which may affect simulation results at low $\delta^{18}O$ (Fig. S2). As an example, in stochastic simulation #6, we assign the transition temperature between liquid and mixed-phase clouds and between mixed-phase and ice clouds at −10 °C and − 40 °C, respectively (Schoenemann and Steig, 2016), to extend the liquid-vapor fractionation to lower temperatures and delay the predominance of ice-vapor fractionation (Fig. S1), while all other conditions are kept the same as in the simplest stochastic simulation #1. The results indicate that the sharp increase of precipitation $\Delta'^{17}O$ for $\delta^{18}O < -20‰$ due to the onset of supersaturation-induced kinetic effects shown in stochastic simulation #1 is no longer present, and there is a closer data-model fit for d-excess as well compared to stochastic simulation #1 (Fig. 13c). However, regardless of the parameterization of ice-vapor fractionation, we find that raindrop re-evaporation/equilibration and vapor mixing are always required in order to achieve a data-model fit in the full range of $\delta^{18}O$.

5.3. Implications of data-model comparison

We conduct a series of stochastic simulations to demonstrate that the two key patterns of precipitation $\delta^{18}O$, d-excess, and $\Delta'^{17}O$ variations in observations can be reasonably captured by the Rayleigh distillation model if raindrop re-evaporation/equilibration and vapor mixing effects are incorporated and a large analytical error for $\Delta'^{17}O$ is assumed. This parsimonious solution implies that other processes affecting d-excess and $\Delta'^{17}O$ are not needed to capture the full range of variability,

although it does not mean that they are not locally or regionally important. This insight is potentially useful for understanding the large-scale fundamental controls of the isotopic variations in global precipitation (Hendricks et al., 2000; Bailey et al., 2018; Putman et al., 2019), uniquely from a constraint of second-order isotopic parameters.

Notably, terrestrial moisture recycling is one of those excluded processes, despite being an important part of the water cycle. Our previous study on d-excess has argued that terrestrial moisture recycling likely possesses a very complex isotopic fingerprint; it is often strongest in the warm and dry season when plant activity and water storage depletion are enhanced, resulting in higher T/ET and, in particular, $P < ET$ conditions (Xia et al., 2022). Under these conditions, evapotranspiration outfluxes may have lower d-excess and $\Delta'^{17}O$ than precipitation influxes and act to decrease the d-excess and $\Delta'^{17}O$ of downwind water vapor and precipitation, as opposed to our limited analysis of δ_{ET} model in Section 4.1 that has only considered $P > ET$ conditions. The fact that terrestrial moisture recycling is not required to capture the overall relationships among $\delta^{18}O$, d-excess, and $\Delta'^{17}O$ implies that its isotopic effect, if any, only has limited spatial and temporal extents, or has limited magnitudes of signals, or is muted by large-scale competing controls of continental water balance between $P > ET$ and $P < ET$ conditions. This idea is consistent with those GCM-based studies, which demonstrate that precipitation d-excess can be reasonably simulated even when evapotranspiration fluxes are set to not fractionate (Risi et al., 2010a; Werner et al., 2011).

6. Discussion and perspectives

6.1. On the commonality and distinction between d-excess and $\Delta'^{17}O$

Although d-excess and $\Delta'^{17}O$ are defined under different mathematical forms (linear δ notation vs. non-linear δ' notation) and their respective amplitudes are identified on different scales (‰ vs. per meg), both in fact simply quantify the deviation relative to the reference relationship of the isotopic composition in average meteoric water as a measure of the scale of diffusion-induced kinetic fractionation. For this, we stress that d-excess and $\Delta'^{17}O$ should first of all be viewed as similar parameters for their common responses in terms of the direction of change to hydroclimate processes that involve kinetic fractionation, such as oceanic evaporation, terrestrial moisture recycling, and raindrop re-evaporation, in which diffusional transports of water vapor across humidity gradients occur. It is feasible to invoke a similar framework for qualitative interpretations of high and low values in these two second-order isotopic parameters (Aron et al., 2021).

In this review, we also show that the sensitivities of d-excess and $\Delta'^{17}O$ to terrestrial moisture recycling and raindrop re-evaporation vary under different conditions. Generally, when kinetic fractionation is stronger and results in larger shifts in both d-excess and $\Delta'^{17}O$, such as in the cases of evaporation-dominated terrestrial moisture recycling or re-evaporation of raindrops in light rains, the magnitude of shifts is relatively larger for $\Delta'^{17}O$ than for d-excess, resulting in a higher $\Delta(\Delta'^{17}O)/\Delta$(d-excess).

Secondly, d-excess and $\Delta'^{17}O$ have different responses to temperature-dependent equilibrium fractionation. This distinction is well known and often discussed in terms of temperature sensitivity during oceanic evaporation; the d-excess of oceanic evaporation fluxes is sensitive to SST but $\Delta'^{17}O$ is not. Thus, combining these two complementary tracers in polar ice-core studies has the potential to deduce independent records of long-term SST and oceanic RH (Angert et al., 2004; Landais et al., 2008; Landais et al., 2012b; Xia, 2023). However, in this review, we stress that the different responses of d-excess and $\Delta'^{17}O$ to equilibrium fractionation are strongly and pervasively expressed in their distinct non-conservative behaviors during condensation and Rayleigh distillation. The 1st type of non-conservative behavior—the shifts of d-excess and $\Delta'^{17}O$ from water vapor to precipitation—act as a source of noise that overprints their signals in water vapor and is partly responsible for the very weak correlation between d-excess and $\Delta'^{17}O$ in precipitation observations. The 2nd type of non-conservative behavior—the shifts of d-excess and $\Delta'^{17}O$ in precipitation throughout Rayleigh distillation—act to dampen the 1st type of non-conservative behavior.

There are also other definitions of these second-order isotopic parameters such as the logarithmic deuterium excess (Uemura et al., 2012; Dütsch et al., 2017) and the excess of ^{17}O relative to a different reference slope (Uechi and Uemura, 2019; Aron et al., 2021). Our data compilation shown in Fig. 11 supports a recently emerging view: because mean precipitation $\Delta'^{17}O$ increases steadily with decreasing precipitation $\delta^{18}O$ among these observational data, the excess term of ^{17}O is more suitable to be defined on a lower reference slope (λ) (Miller, 2018; Aron et al., 2023). Based on our compiled $\Delta'^{17}O$ database, we here use the linear regression to derive a new triple oxygen isotope meteoric water line for the range of $\delta^{18}O$ from −25‰ to −2‰ as:

$$\delta'^{17}O\ (‰) = 0.5272 \times \delta'^{18}O + 0.020. \quad (8)$$

Eq. (8) means that $\lambda = 0.5272$ should be seriously considered for the possible new definition of $\Delta'^{17}O$ for hydrological studies in the future. This value is higher than those proposed previously by others (0.5264–0.5268) (Sharp et al., 2018; Aron et al., 2021; Aron et al., 2023). In addition to that this database has included to our knowledge the complete published datasets to date, our λ value is uniquely free from biases of both polar precipitation data (with very low $\delta^{18}O$) and—more importantly—other data strongly affected by raindrop re-evaporation based on the emerging pattern of d-excess (that do diverge from the mean value of 10‰ for $\delta^{18}O > -2‰$). Regardless, we stress that these alternative definitions for d-excess and $\Delta'^{17}O$ do not change their purposes for measuring isotopic deviations relative to a given reference. They also do not impact our understanding of the commonality and distinction between these two parameters.

6.2. Opportunities, challenges, and directions

By interrogating the similarities and differences between d-excess and $\Delta'^{17}O$ dynamics, we suggest several future opportunities to leverage the joint information from precipitation d-excess and $\Delta'^{17}O$ data to fingerprint water cycle processes.

First, combining d-excess and $\Delta'^{17}O$ data has the potential to inversely estimate the independent signals of SST and oceanic RH prevailing at the oceanic moisture source. It is the most well-known application in ice-core records, with increased availability of new $\Delta'^{17}O$ data to complement traditional d-excess records (Angert et al., 2004; Landais et al., 2008; Landais et al., 2012b; Landais et al., 2018; Steig et al., 2021). However, we note the complication that the independent SST signal might be overprinted by the short-term variability in other factors at the boundary layer that also affect the d-excess and $\Delta'^{17}O$ of oceanic vapor, not to mention processes during vapor transport and condensation (Schoenemann et al., 2014; Li et al., 2015). Therefore, the application must consider on what timescale the independent SST effect can be distinguished from noisy isotope data (Xia, 2023).

Second, $\Delta'^{17}O$ is a more sensitive tracer than d-excess for fingerprinting terrestrial hydroclimate processes that involve strong kinetic fractionation such as tracking the surface evaporation flux in moisture recycling or detecting the re-evaporation of light rains. In addition, $\Delta'^{17}O$ is insensitive to temperature-dependent equilibrium fractionation as reflected by the stable non-conservative behavior during liquid condensation (always shift by about 10 per meg) and Rayleigh distillation (varies very little across distillation profiles), as opposed to d-excess. This further makes $\Delta'^{17}O$ a tracer uniquely diagnostic of kinetic fractionation in terrestrial hydroclimate processes when the temperature is above the freezing point. To this end, combining paired d-excess and $\Delta'^{17}O$ data may provide an important avenue to disentangle the isotopic fingerprint of oceanic and terrestrial processes (Xia et al., 2022;

Xia, 2023).

Third, when the temperature is below the freezing point, precipitation $\Delta'^{17}O$ is highly sensitive to the balance between kinetic fractionation in ice condensation that increases $\Delta'^{17}O$ and vapor mixing that decreases $\Delta'^{17}O$, while precipitation d-excess responds slightly to both effects. This makes combining snow d-excess and $\Delta'^{17}O$ data not only useful to constrain the degree of supersaturation of water vapor over ice in cold clouds (Risi et al., 2013; Schoenemann et al., 2014; Schoenemann and Steig, 2016), but also to characterize atmospheric mixing.

Despite these emerging opportunities, the present challenge is that both d-excess and $\Delta'^{17}O$ are complex and opaque tracers. Their values measured in a precipitation sample represent the aggregation of multiple fractionation processes at the moisture source (oceanic evaporation), en route (Rayleigh distillation, vapor mixing, and terrestrial moisture recycling), and at the moisture sink (raindrop re-evaporation/equilibration and ice condensation in supersaturation conditions) (Risi et al., 2013; Xia et al., 2022; Aron et al., 2023). Quantifying and understanding the role of each fractionation process that is likely spatially- and timescale-dependent is essential for an accurate interpretation of these tracers, in particular for $\Delta'^{17}O$ that can be measured in various geological materials in the future. Recent work has made progress towards this goal, for example, by using moisture tracking models to quantify the d-excess and $\Delta'^{17}O$ of oceanic source vapor (Xia et al., 2022; Xia, 2023). Specifically, it is demonstrated that oceanic moisture source conditions are not the dominant control of seasonal changes in precipitation d-excess in low-latitudes and are locally overprinted by local raindrop re-evaporation/equilibration (Xia et al., 2022).

Over longer timescales, d-excess and $\Delta'^{17}O$ data from paleoclimate archives are sparse and almost exclusively provided by ice cores. Interpretations of their temporal variations preserved in these archives often invoke one specific process or mechanism without considering the complexity of aggregating multiple processes or mechanisms. For example, the d-excess and $\Delta'^{17}O$ variations in ice cores are often attributed to changes in oceanic evaporation conditions (Vimeux et al., 1999; Landais et al., 2008; Risi et al., 2010b; Winkler et al., 2012; Shao et al., 2021), whereas some studies recognize the important role of local supersaturation-induced kinetic effects in snow formation (Winkler et al., 2012; Schoenemann et al., 2014; Pang et al., 2015). For other archives, a study on speleothem paleo-fluid inclusions in the western Amazon rainforest has documented precipitation d-excess variations of 7‰ during the Holocene, which coincide with changes in tree pollen abundance and likely reflect the strength of terrestrial moisture recycling in response to past hydroclimate and vegetation changes (van Breukelen et al., 2008; Ampuero et al., 2020). More recently, Sha et al. (2020) have developed an approach for measuring speleothem carbonate $\Delta'^{17}O$ to reconstruct paleo-precipitation $\Delta'^{17}O$ and tentatively interpreted their records during the late Quaternary, including from a site in the western Amazon rainforest, as reflecting oceanic evaporation conditions.

To bridge the current knowledge gap about the multiple, compound controls of precipitation d-excess and $\Delta'^{17}O$, we suggest that site-specific, multiple-year 12 monthly means of paired precipitation d-excess and $\Delta'^{17}O$ data are most useful to understand the common and distinct isotopic patterns in these two parameters, to disentangle the contribution of each fractionation process, and to develop an interpretive framework for their variations preserved in geological records (Aron et al., 2023). These intermediate-timescale precipitation isotope data average out the short-term isotopic variability in precipitation related to synoptic and mesoscale conditions, are long enough to "measure" the isotopic characteristics of precipitation produced at a range of climate conditions in different seasons, and are practical to collect within a few years' efforts for building a benchmark. Our previous work has examined the 12 monthly means of precipitation d-excess data from GNIP stations worldwide and provided a synopsis of their controlling factors in different regions (Xia et al., 2022). The same analysis can be extended to $\Delta'^{17}O$ when data become available. Recently, Aron et al. (2023) showed a consistent pattern that precipitation $\Delta'^{17}O$ is higher in winter and lower in summer across the conterminous US but not so in d-excess data. From the insights gained from the analysis of theoretical models, we suggest that the more sensitive response of $\Delta'^{17}O$ to terrestrial hydroclimate processes, the larger increase of $\Delta'^{17}O$ in ice condensation (strongly increased winter precipitation $\Delta'^{17}O$), and the complication of equilibrium fractionation for d-excess in condensation and Rayleigh distillation, are three potential reasons for that finding.

Finally, with regard to geological applications of triple oxygen isotope techniques, many paleo-archives are formed with surface water in an evaporative environment (e.g., lakes, soils) and are prone to evaporative enrichment of heavy isotope species in surface water (Evans et al., 2018; Gázquez et al., 2018; Beverly et al., 2021; Passey and Levin, 2021). These processes are frequently imprinted in geological records but are not considered in this review that is aimed to understand the hydroclimate processes and mechanisms responsible for isotopic variations in precipitation. Additionally, the d-excess and $\Delta'^{17}O$ of ocean water also vary in the past, the fact that need to be considered in a quantitative analysis of paleo-isotope data (Stenni et al., 2001; Kelson et al., 2022).

Declaration of Competing Interest

The authors declare that they have no known competing financial interests or personal relationships that could have appeared to influence the work reported in this paper.

Data availability

All data synthesized here are available in cited original studies as tabular data except three studies, which can be accessed by contacting the authors of original studies or digitizing their figures.

Acknowledgments

We thank Stéphane Affolter and Markus Leuenberger for providing their data. This work was supported by the "Fundamental Research Funds for the Central Universities" (135112004) to ZX, the PRIME program of the German Academic Exchange Service (DAAD) to JS, and a UMass Faculty Startup Fund to MJW. ZX is indebted to Lijian Wang and Zicheng Yu, who provided him with tremendous support during a period of personal hardships when this study was conducted. All model codes related to this work are made available on a GitHub repository (https://github.com/zhx215/dxsD17O).

Appendix A. Theoretical relationship between Δ(d-excess) and Δ($\Delta'^{17}O$) in kinetic fractionation

For a simple isotopic fractionation in which substance B is derived from substance A, its isotopic composition ($^{X}\delta_B$) follows:

$$^{X}\delta_B\ (‰) = \left(^{X}\delta_A + 1000\right)^{X}\alpha - 1000, \tag{A1}$$

where $^{X}\delta_A$ is the isotopic composition of substance A (in ‰) and $^{X}\alpha$ denotes the fractionation factor. For water isotopologues, X denotes the individual

heavy isotope species (2 for ^{2}H, 18 for ^{18}O, 17 for ^{17}O). Eq. (A1) may represent the equilibrium fractionation in water phase change (chemical reaction) or the kinetic fractionation in water vapor diffusion (physical transport). In the latter case, vapor B is directly derived by diffusional transport from vapor A across a humidity gradient of 100%. The Δ(d-excess) and Δ($\Delta'^{17}O$) between B and A (Δ > 0 means a higher value in B than A) are:

$$\Delta(\mathrm{d-excess})\ (‰) = \left({}^{2}\delta_A + 1000\right)\left({}^{2}\alpha - 1\right) - 8 \times \left({}^{18}\delta_A + 1000\right)\left({}^{18}\alpha - 1\right) \tag{A2}$$

and

$$\Delta\left(\Delta'^{17}O\right)\ (\mathrm{per\ meg}) = \left[ln\left({}^{17}\alpha\right) - 0.528 \times ln\left({}^{18}\alpha\right)\right] \times 10^{6}, \tag{A3}$$

respectively. For kinetic fractionation, ${}^{X}\alpha$ is empirically expressed as $({}^{X}D'/{}^{X}D)^{m}$ where ${}^{X}D'/{}^{X}D$ is the ratio of diffusion coefficients of the heavy over the light isotope species, which is 0.9757 for $^{2}H/^{1}H$, 0.9727 for $^{18}O/^{16}O$, and $(0.9727)^{0.518} = 0.9858$ for $^{17}O/^{16}O$ (Merlivat, 1978; Barkan and Luz, 2007), and m is the aerodynamic exponent that in theory ranges from 0 for pure turbulence (no kinetic fractionation involved) to 1 for pure molecular diffusion. These ${}^{X}D'/{}^{X}D$ values have been confirmed by recent advanced kinetic theory calculations with very weak temperature sensitivity as well as by laboratory experiments, although the value for $^{18}O/^{16}O$ may have an unknown offset of 0.02 (Hellmann and Harvey, 2020; Pierchala et al., 2022). By further assuming that ${}^{18}\delta_A$ ranges from −30‰ to 0‰ and ${}^{2}\delta_A - 8\times {}^{18}\delta_A$ ranges from −20‰ to 40‰, which are reasonable values in modern meteoric water, Δ($\Delta'^{17}O$)/Δ(d-excess) is calculated to be between 1.40 and 1.44.

Appendix B. Effective fractionation factor in condensation

The effective fractionation factor (${}^{X}\alpha_{eff}$) during condensation is represented by liquid-vapor equilibrium fractionation factor (${}^{X}\alpha_{eq}^{l-v}$) for $T_d \geq 0$ °C, a combination of ice-vapor equilibrium fractionation factor (${}^{X}\alpha_{eq}^{i-v}$) and kinetic fractionation factor due to supersaturation of water vapor over ice (${}^{X}\alpha_{k}^{i-v}$) for $T_d \leq -23$ °C (Jouzel and Merlivat, 1984), and is interpolated cubically between $T_d = -23$ °C and 0 °C when $-23\ °C < T_d < 0\ °C$ to approximate mixed-phase conditions (Dütsch et al., 2017). The equations to derive ${}^{X}\alpha_{eff}$ are:

$${}^{X}\alpha_{eff} = \begin{cases} {}^{X}\alpha_{eq}^{l-v}, T_d \geq 0°C \\ b_1(T_d + 273.15)^3 + b_2(T_d + 273.15)^2 + b_3(T_d + 273.15) + b_4,\ -23°C < T_d < 0°C, \\ {}^{X}\alpha_{eq}^{i-v} \times {}^{X}\alpha_{k}^{i-v}, T_d \leq -23°C \end{cases} \tag{B1}$$

where

$${}^{X}\alpha_{eq}^{l-v} = exp\left[\frac{a_1}{(T_d + 273.15)^2} + \frac{a_2}{T_d + 273.15} + a_3\right], \tag{B2}$$

$${}^{X}\alpha_{eq}^{i-v} = exp\left[\frac{c_1}{T_d + 273.15} + c_2\right], \tag{B3}$$

and

$${}^{X}\alpha_{k}^{i-v} = \frac{S_i}{{}^{X}\alpha_{eq}^{i-v}\left(\frac{{}^{X}D'}{{}^{X}D}\right)^{-1}(S_i - 1) + 1}. \tag{B4}$$

The S_i expresses the supersaturation of water vapor over ice as:

$$S_i = 1 - \lambda T_d, \tag{B5}$$

where we assume $\lambda = 0.004$ (Risi et al., 2013). The coefficients in Eqs. (B1)–(B3) for deriving ${}^{2}\alpha_{eff}$ and ${}^{18}\alpha_{eff}$ are (Merlivat and Nief, 1967; Majoube, 1971b; Majoube, 1971a):

$$\begin{cases} a_1 = 24844 \\ a_2 = -76.248 \\ a_3 = 0.05261 \\ b_1 = 2.252148 \times 10^{-6} \\ b_2 = -0.001771881 \\ b_3 = 0.4623108 \\ b_4 = -38.86489 \\ c_1 = 16289 \\ c_2 = -0.0945 \end{cases} \tag{B6}$$

and

$$\begin{cases} a_1 = 1137 \\ a_2 = -0.4156 \\ a_3 = -0.00207 \\ b_1 = 3.409942 \times 10^{-7} \\ b_2 = -2.697236 \times 10^{-4} \\ b_3 = 0.07091766 \\ b_4 = -5.184572 \\ c_1 = 11.839 \\ c_2 = -0.028224 \end{cases}, \tag{B7}$$

respectively. These equations for ${}^{X}\alpha_{eq}^{l-v}$ and ${}^{X}\alpha_{eq}^{i-v}$ determined decades ago are still in use for their accuracy, but there exists a very different equation for ${}^{2}\alpha_{eq}^{i-v}$ (Ellehoj et al., 2013), which is however disputed (Lamb et al., 2017). To derive ${}^{17}\alpha_{eff}$ from Eqs. (B1)–(B3), the ${}^{18}\alpha_{eq}^{l-v}$, ${}^{18}\alpha_{eq}^{i-v}$, ${}^{18}D'/{}^{18}D$ values are replaced by $({}^{18}\alpha_{eq}^{l-v})^{0.529}$, $({}^{18}\alpha_{eq}^{i-v})^{0.529}$, and $({}^{18}D'/{}^{18}D)^{0.518}$ based on the power law relationship in mass-dependent equilibrium and kinetic fractionation (Barkan and Luz, 2005; Barkan and Luz, 2007). The coefficients for interpolated mixed-phase conditions are:

$$\begin{cases} b_1 = 1.833597 \times 10^{-7} \\ b_2 = -1.44968 \times 10^{-4} \\ b_3 = 0.03809801 \\ b_4 = -2.320959 \end{cases}. \tag{B8}$$

The values for ${}^{X}D'/{}^{X}D$ are provided in Appendix A. The plots for the relationship between ${}^{X}\alpha_{\text{eff}}$ and T_d are shown in Fig. S1.

Appendix C. The new model for δ_{ET} with water storage and runoff terms

The model for the isotopic composition of evapotranspiration fluxes (${}^{X}\delta_{ET}$) is developed following two assumptions: (1) a closure assumption is applied to model isotopic fluxes from terrestrial evaporation analogous to Eq. (2) but the isotopic composition of the boundary layer vapor is also filled partially by the concurrent transpiration flux depending on transpiration fraction T/ET (Aemisegger et al., 2014); and (2) the removal of liquid source water by the evapotranspiration outflux follows a Rayleigh-type process (Caves et al., 2015). The following is derived (Xia and Winnick, 2021):

$${}^{X}\delta_{ET}\ (‰) = \left(1 - \frac{T}{ET}\right)\frac{\int_1^F \left[{}^{X}\alpha_{ET}\left({}^{X}\delta_s + 1000\right)F^{{}^{X}\alpha_{ET}-1} - 1000\right]\mathrm{d}F}{F-1} + \left(\frac{T}{ET}\right){}^{X}\delta_s, \tag{C1}$$

where ${}^{X}\alpha_{ET}$ is the apparent fractionation factor of evaporation affected by transpiration, F is the remaining fraction of source water after the evapotranspiration outflux, and ${}^{X}\delta_s$ is the isotopic composition of source water (in ‰). The ${}^{X}\alpha_{ET}$ is calculated as (Xia and Winnick, 2021):

$${}^{X}\alpha_{ET} = \left(1 - \frac{T}{ET}\right)\left\{\frac{\left(\frac{{}^{X}D'}{{}^{X}D}\right)^{m}{}^{X}\alpha_{eq}^{l-v-1}}{\left(1 - \frac{h}{100}\right)\left[1 + \left(\frac{{}^{X}D'}{{}^{X}D}\right)^{m}\left(1 - \frac{T}{ET}\right)\left(\frac{h}{100-h}\right)\right]}\right\} + \left(\frac{T}{ET}\right)\left[\frac{1}{1 + \left(\frac{{}^{X}D'}{{}^{X}D}\right)^{m}\left(1 - \frac{T}{ET}\right)\left(\frac{h}{100-h}\right)}\right], \tag{C2}$$

where h is the surface RH (in %) and ${}^{X}\alpha_{eq}^{l-v}$ is the liquid-vapor equilibrium fractionation factor at surface temperature. The aerodynamic exponent m ranges between 0.5 and 1 after assuming $\Theta = 1$ (see Section 2) adapted for terrestrial environments (Gat, 1996). In our previous work (Xia and Winnick, 2021), precipitation is the only source water for evapotranspiration and $F = (P - ET)/P$. In this study, simple runoff and water storage terms are incorporated. Then, ${}^{X}\delta_s$ is the mass-weighted mean of the isotopic compositions of water storage (${}^{X}\delta_{ws}$) and precipitation (${}^{X}\delta_p$) as:

$${}^{X}\delta_s\ (‰) = \frac{S \bullet {}^{X}\delta_{ws} + P \bullet {}^{X}\delta_p}{S + P} = \frac{{}^{X}\delta_{ws}}{1 + \left(\frac{S}{P}\right)^{-1}} + \frac{{}^{X}\delta_p}{1 + \frac{S}{P}}, \tag{C3}$$

where S/P represents the size of water storage available for mixing and evapotranspiration relative to the precipitation influx. This ratio is complex in nature and related to a range of geological, climatic, and ecological factors (Xia et al., 2022). Globally, this ratio is estimated to be about 0.2 (Güntner et al., 2007), but it could be much higher in groundwater-dependent ecosystems. The F is modified as:

$$F = \frac{S}{S + ET} = \frac{1}{1 + \frac{ET}{P}\left(\frac{S}{P}\right)^{-1}}, \tag{C4}$$

where ET/P represents the water balance. To compute ${}^{X}\delta_{ET}$ from Eqs. (C1)–(C4), only ${}^{X}\delta_{ws}$ remains unknown. At isotopic steady state, ${}^{X}\delta_{ws}$ equals the isotopic composition of residual water storage after the source water is removed by the evapotranspiration outflux. A simple isotopic mass balance yields:

$${}^{X}\delta_{ws}\ (‰) = \frac{(ET + S) \bullet {}^{X}\delta_s - ET \bullet {}^{X}\delta_{ET}}{S} = \left[1 + \frac{ET}{P}\left(\frac{S}{P}\right)^{-1}\right]{}^{X}\delta_s - \left[\frac{ET}{P}\left(\frac{S}{P}\right)^{-1}\right]{}^{X}\delta_{ET}. \tag{C5}$$

By combining Eqs. (C1), (C3), and (C5), both ${}^{X}\delta_{ws}$ and ${}^{X}\delta_s$ can be eliminated to derive an analytical expression for ${}^{X}\delta_{ET}$ that only requires ${}^{X}\delta_p$ as an isotopic input term. Alternatively, ${}^{X}\delta_{ET}$ can be obtained numerically by approximating the unique ${}^{X}\delta_{ws}$ value that satisfies Eqs. (C1), (C3), and (C5) at once.

Appendix D. The reactive transport model for δ_v with moisture recycling

Hendricks et al. (2000) developed an isotope-enabled reactive transport model for water vapor that allows for moisture cycling. The model can be simplified with respect to dimensionless distance and the analytical solution for advective transport has a similar formulation to the Rayleigh distillation equation as (Winnick et al., 2014):

$$^{X}\delta_{v}\ (‰) = \left(^{X}\delta_{v,0} - {}^{X}\delta_{v}^{\infty}\right) f^{{}^{X}\alpha_{eff} + {}^{X}\alpha_{eff} \bullet N_d - 1} + \delta_{v}^{\infty}, \tag{D1}$$

where

$$\delta_{v}^{\infty}\ (‰) = \frac{N_d \bullet {}^{X}\delta_{ET} - (1 + N_d)\left({}^{X}\alpha_{eff} - 1\right)1000}{{}^{X}\alpha_{eff} + {}^{X}\alpha_{eff} \bullet N_d - 1} \tag{D2}$$

and

$$N_d\ (\text{Damköhler number}) = \frac{ET}{P - ET} = \frac{1}{\left(\frac{ET}{P}\right)^{-1} - 1}. \tag{D3}$$

This model incorporates the feedback of moisture recycling through the term $^{X}\delta_{ET}$ to modulate the isotopic evolution of water vapor. The isotopic composition of precipitation, $^{X}\delta_{p}$, is obtained by Eq. (6). Note that f here is interpreted as the net degree of distillation. When $N_d = 0$ (no moisture recycling), Eq. (D1) reduces to the Rayleigh distillation equation, i.e., Eq. (4).

Appendix E. The Stewart model

The static raindrop re-evaporation model of Stewart (1975) is developed from Fick's law that underpins the Craig and Gordon (1965) model, with the difference that the Stewart (1975) model represents raindrop re-evaporation as a Rayleigh-type progressive removal of liquid and includes evaporation amount as a model input (Gonfiantini et al., 2018). By assuming that the ambient water vapor is in isotopic equilibrium with the initial raindrop, the Stewart (1975) model is expressed as follows in order to obtain the isotopic composition of the final, evaporated raindrop (Liebminger et al., 2006):

$$^{X}\delta_{d}\ (‰) = {}^{X}\delta_{d,0} + \left[(1 - E)^{{}^{X}\beta} - 1\right]\left({}^{X}\delta_{d,0} + 1000\right)\left(1 - \frac{{}^{X}\gamma}{{}^{X}\alpha_{eq}^{l-v}}\right), \tag{E1}$$

with

$$^{X}\beta = \frac{1 - {}^{X}\alpha_{eq}^{l-v}\left(\frac{{}^{X}D'}{{}^{X}D}\right)^{-m}\left(1 - \frac{h_d}{100}\right)}{{}^{X}\alpha_{eq}^{l-v}\left(\frac{{}^{X}D'}{{}^{X}D}\right)^{-m}\left(1 - \frac{h_d}{100}\right)} \tag{E2}$$

and

$$^{X}\gamma = \frac{{}^{X}\alpha_{eq}^{l-v}\left(\frac{h_d}{100}\right)}{1 - {}^{X}\alpha_{eq}^{l-v}\left(\frac{{}^{X}D'}{{}^{X}D}\right)^{-m}\left(1 - \frac{h_d}{100}\right)}, \tag{E3}$$

where $^{X}\delta_{d}$ and $^{X}\delta_{d,0}$ are the isotopic compositions of the final and initial raindrop (in ‰), respectively, E is the fraction of evaporative loss, $^{X}\alpha_{eq}^{l-v}$ is the liquid-vapor equilibrium fractionation factor at raindrop temperature, and h_d is the RH of ambient atmosphere with respect to saturation vapor pressure at raindrop temperature (in %). The aerodynamic exponent m for raindrops was determined as 0.58 in laboratory experiments (Stewart, 1975). This model has been applied in a number of studies to quantify the effect of raindrop re-evaporation on the isotopic composition of precipitation after assuming or estimating the raindrop temperature, raindrop RH, and evaporation amount (Liebminger et al., 2006; Froehlich et al., 2008; Kong et al., 2013; Wang et al., 2016b). To demonstrate the model behavior, we run this static model for a hypothetical raindrop over a range of raindrop temperatures and raindrop RH at three evaporation fraction values at 0.05, 0.2, and 0.35. The results are shown in Fig. S5.

Appendix F. Model inputs and sampling procedures for stochastic simulations of pseudo-precipitation

We download ERA5 single-level reanalysis monthly fields of 0.25° × 0.25° resolution and extract 12 monthly means of relevant parameters from 1981 to 2010 (Hersbach et al., 2020). For ocean grids (sea ice excluded), we derive the joint probability distribution of oceanic RH and T_d (i.e., the dew temperature field) weighted by latent heat flux and grid area separately for 12 months and two hemispheres. For land grids, we similarly derive the probability distribution of T_d weighted by precipitation flux and grid area. We also download the output of the isotope-enabled GCM LMDZ4 simulation from 1994 to 2010 (monthly product) and derive the probability distribution of lowest-level vapor $\delta^{18}O$ for each T_d over ocean grids (without distinguishing the month and hemisphere due to coarse grid resolution). This GCM is the only one archived in the Stable Water Isotope Intercomparison Group Phase 2 (SWING2) project that has the accessible output of model parameters required to derive the probabilistic relationship between oceanic vapor $\delta^{18}O$ and T_d (Risi et al., 2012).

To simulate the isotopic composition of each pseudo-precipitation, first, a pair of oceanic RH and T_d is randomly sampled from their summed (over

12 months and two hemispheres) joint probability distribution (Figs. S6a–c). At the same time, we tag the month and hemisphere from which that sample is actually taken. Next, the oceanic vapor d-excess and $\Delta'^{17}O$ are randomly sampled independently based on the oceanic RH using their empirical linear relationships and prediction intervals (i.e., Fig. 2a and b; note that we use the prediction interval of $\Delta'^{17}O$ after discounting the analytical error). Then, the oceanic vapor $\delta^{18}O$ is randomly sampled according to its LMDZ4-based probability distribution at the oceanic T_d (Fig. S6d). This procedure is aimed to find a reasonable oceanic vapor $\delta^{18}O$ value given a particular T_d, as recommended by Jouzel and Koster (1996). These are the initial condition inputs needed for the simulation. After that, the continental T_d, the only final condition input needed for the simulation, is randomly sampled from its probability distribution in the same month and hemisphere as the sample of the initial condition (Fig. S6e). The reason for sampling the initial and final conditions in the same month and hemisphere is to ensure that the simulation is at least realistic in climatology (e.g., oceanic evaporation in winter conditions is unlikely the moisture source for summer precipitation). Finally, the Rayleigh distillation profile is established starting from the initial condition at the oceanic moisture source to the final condition at the continental moisture sink if there is a gradient of decreasing T_d (otherwise that simulation is skipped). The isotopic composition of pseudo-precipitation at the end of the distillation profile is the output of the simulation. Note that for each simulation, the precipitation $\Delta'^{17}O$ value is resampled with a normally distributed perturbation of ±5 per meg (1σ) to represent the least analytical error in triple oxygen isotope measurements (Luz and Barkan, 2010). This stochastic simulation procedure is repeated 10^6 times to derive a synthetic dataset of the isotopic composition of precipitation. We note that as the probability distributions of initial and final conditions are flux-weighted, moisture sources with high evaporation fluxes such as subtropical oceans and moisture sinks with high precipitation fluxes such as tropical rainforests will be overrepresented in the synthetic dataset.

The procedure described above is for the simplest scenario, i.e., the stochastic simulation #1 in Section 5.2. This Rayleigh distillation-based forward model and its sampling procedure can be made more complex by incorporating other processes such as terrestrial moisture recycling, raindrop re-evaporation/equilibration, and vapor mixing. As for incorporating the raindrop re-evaporation effect presented in Section 5.2, ERA5-based surface temperatures at oceanic moisture sources and continental moisture sinks are additionally sampled from their probability distributions versus T_d (e.g., Fig. S6f). The surface RH gradient across the distillation profile is calculated from surface temperature and T_d gradients (Bolton, 1980). Raindrop diameter is sampled between 0.4 mm and 2.6 mm. Then, surface temperature, surface RH, and raindrop diameter together determine the fractionation factor ($^{X}\alpha_{RR}$) associated with raindrop re-evaporation, which is incorporated into the Rayleigh distillation-based forward model by replacing $^{X}\alpha_{eff}$ with $^{X}\alpha_{eff} \cdot {}^{X}\alpha_{RR}$ (Xia and Winnick, 2021). If the raindrop has been completely evaporated due to the small diameter and low surface RH before reaching the end of the profile, that simulation is skipped.

Appendix G. Supplementary data

Supplementary data to this article can be found online at https://doi.org/10.1016/j.earscirev.2023.104432.

References

Aemisegger, F., Pfahl, S., Sodemann, H., Lehner, I., Seneviratne, S.I., Wernli, H., 2014. Deuterium excess as a proxy for continental moisture recycling and plant transpiration. Atmos. Chem. Phys. 14, 4029–4054. https://doi.org/10.5194/acp-14-4029-2014.

Aemisegger, F., Sjolte, J., 2018. A climatology of strong large-scale ocean evaporation events. Part II: Relevance for the deuterium excess signature of the evaporation flux. J. Clim. 31, 7313–7336. https://doi.org/10.1175/JCLI-D-17-0592.1.

Ampuero, A., Stríkis, N.M., Apaéstegui, J., Vuille, M., Novello, V.F., Espinoza, J.C., Cruz, F.W., Vonhof, H., Mayta, V.C., Martins, V.T.S., Cordeiro, R.C., Azevedo, V., Sifeddine, A., 2020. The forest effects on the isotopic composition of rainfall in the northwestern Amazon basin. J. Geophys. Res. Atmos. 125,, e2019JD031445 https://doi.org/10.1029/2019JD031445.

Angert, A., Rachmilevitch, S., Barkan, E., Luz, B., 2003. Effects of photorespiration, the cytochrome pathway, and the alternative pathway on the triple isotopic composition of atmospheric O_2. Glob. Biogeochem. Cycles 17, 1030. https://doi.org/10.1029/2002GB001933.

Angert, A., Cappa, C.D., DePaolo, D.J., 2004. Kinetic ^{17}O effects in the hydrologic cycle: indirect evidence and implications. Geochim. Cosmochim. Acta 68, 3487–3495. https://doi.org/10.1016/j.gca.2004.02.010.

Aron, P.G., Levin, N.E., Beverly, E.J., Huth, T.E., Passey, B.H., Pelletier, E.M., Poulsen, C. J., Winkelstern, I.Z., Yarian, D.A., 2021. Triple oxygen isotopes in the water cycle. Chem. Geol. 565, 120026 https://doi.org/10.1016/j.chemgeo.2020.120026.

Aron, P.G., Li, S., Brooks, J.R., Welker, J.M., Levin, N.E., 2023. Seasonal variations in triple oxygen isotope ratios of precipitation in the western and Central United States. Paleoceanog. Paleoclimatol. 38, e2022PA004458 https://doi.org/10.1029/2022PA004458.

Bailey, A., Posmentier, E., Feng, X., 2018. Patterns of evaporation and precipitation drive global isotopic changes in atmospheric moisture. Geophys. Res. Lett. 45, 7093–7101. https://doi.org/10.1029/2018GL078254.

Barkan, E., Luz, B., 2005. High precision measurements of $^{17}O/^{16}O$ and $^{18}O/^{16}O$ ratios in H_2O. Rapid Commun. Mass Spectrom. 19, 3737–3742. https://doi.org/10.1002/rcm.2250.

Barkan, E., Luz, B., 2007. Diffusivity fractionations of $H_2^{16}O/H_2^{17}O$ and $H_2^{16}O/H_2^{18}O$ in air and their implications for isotope hydrology. Rapid Commun. Mass Spectrom. 21, 2999–3005. https://doi.org/10.1002/rcm.3180.

Barnes, C.J., Allison, G.B., 1983. The distribution of deuterium and ^{18}O in dry soils: 1. Theory. J. Hydrol. 60, 141–156. https://doi.org/10.1016/0022-1694(83)90018-5.

Benetti, M., Reverdin, G., Pierre, C., Merlivat, L., Risi, C., Steen-Larsen, H.C., Vimeux, F., 2014. Deuterium excess in marine water vapor: dependency on relative humidity and surface wind speed during evaporation. J. Geophys. Res. Atmos. 119, 584–593. https://doi.org/10.1002/2013JD020535.

Benetti, M., Aloisi, G., Reverdin, G., Risi, C., Sèze, G., 2015. Importance of boundary layer mixing for the isotopic composition of surface vapor over the subtropical North Atlantic Ocean. J. Geophys. Res. Atmos. 120, 2190–2209. https://doi.org/10.1002/2014JD021947.

Bershaw, J., Hansen, D.D., Schauer, A.J., 2020. Deuterium excess and ^{17}O-excess variability in meteoric water across the Pacific Northwest, USA. Tellus B 72, 1–17. https://doi.org/10.1080/16000889.2020.1773722.

Beverly, E.J., Levin, N.E., Passey, B.H., Aron, P.G., Yarian, D.A., Page, M., Pelletier, E.M., 2021. Triple oxygen and clumped isotopes in modern soil carbonate along an aridity gradient in the Serengeti, Tanzania. Earth Planet. Sci. Lett. 567, 116952 https://doi.org/10.1016/j.epsl.2021.116952.

Bolton, D., 1980. The computation of equivalent potential temperature. Mon. Weather Rev. 108, 1046–1053. https://doi.org/10.1175/1520-0493(1980)108<1046:TCOEPT>2.0.CO;2.

Bonne, J.-L., Behrens, M., Meyer, H., Kipfstuhl, S., Rabe, B., Schönicke, L., Steen-Larsen, H.C., Werner, M., 2019. Resolving the controls of water vapour isotopes in the Atlantic sector. Nat. Commun. 10, 1632. https://doi.org/10.1038/s41467-019-09242-6.

Bony, S., Risi, C., Vimeux, F., 2008. Influence of convective processes on the isotopic composition ($\delta^{18}O$ and δD) of precipitation and water vapor in the tropics: 1. Radiative-convective equilibrium and Tropical Ocean-Global Atmosphere–Coupled Ocean-Atmosphere Response Experiment (TOGA-COARE) simulations. J. Geophys. Res. Atmos. 113, D19305 https://doi.org/10.1029/2008JD009942.

Caves, J.K., Winnick, M.J., Graham, S.A., Sjostrom, D.J., Mulch, A., Chamberlain, C.P., 2015. Role of the westerlies in Central Asia climate over the Cenozoic. Earth Planet. Sci. Lett. 428, 33–43. https://doi.org/10.1016/j.epsl.2015.07.023.

Chamberlain, C.P., Ibarra, D.E., Lloyd, M.K., Kukla, T., Sjostrom, D., Gao, Y., Sharp, Z.D., 2020. Triple oxygen isotopes of meteoric hydrothermal systems – implications for palaeoaltimetry. Geochem. Perspect. Lett. 15, 6–9. https://doi.org/10.7185/geochemlet.2026.

Craig, H., 1961. Isotopic variations in meteoric waters. Science 133, 1702–1703. https://doi.org/10.1126/science.133.3465.1702.

Craig, H., Gordon, L.I., 1965. Deuterium and oxygen 18 variations in the ocean and the marine atmosphere. In: Tongiorgi, E. (Ed.), Stable Isotopes in Oceanographic Studies and Paleotemperatures. Consiglio nazionale delle Ricerche, Laboratorio di Geologia Nucleare, Pisa, Italy, pp. 9–130.

Dansgaard, W., 1964. Stable isotopes in precipitation. Tellus 16, 436–468. https://doi.org/10.3402/tellusa.v16i4.8993.

Dütsch, M., Pfahl, S., Sodemann, H., 2017. The impact of nonequilibrium and equilibrium fractionation on two different deuterium excess definitions. J. Geophys. Res. Atmos. 122, 12732–12746. https://doi.org/10.1002/2017JD027085.

Dütsch, M., Blossey, P.N., Steig, E.J., Nusbaumer, J.M., 2019. Nonequilibrium fractionation during ice cloud formation in iCAM5: evaluating the common parameterization of supersaturation as a linear function of temperature. J. Adv. Model. Earth Syst. 11, 3777–3793. https://doi.org/10.1029/2019MS001764.

Ellehoj, M.D., Steen-Larsen, H.C., Johnsen, S.J., Madsen, M.B., 2013. Ice-vapor equilibrium fractionation factor of hydrogen and oxygen isotopes: experimental investigations and implications for stable water isotope studies. Rapid Commun. Mass Spectrom. 27, 2149–2158. https://doi.org/10.1002/rcm.6668.

Evans, N.P., Bauska, T.K., Gázquez-Sánchez, F., Brenner, M., Curtis, J.H., Hodell, D.A., 2018. Quantification of drought during the collapse of the classic Maya civilization. Science 361, 498–501. https://doi.org/10.1126/science.aas9871.

Froehlich, K., Kralik, M., Papesch, W., Rank, D., Scheifinger, H., Stichler, W., 2008. Deuterium excess in precipitation of Alpine regions – moisture recycling. Isot. Environ. Health Stud. 44, 61–70. https://doi.org/10.1080/10256010801887208.

Gat, J.R., Matsui, E., 1991. Atmospheric water balance in the Amazon basin: an isotopic evapotranspiration model. J. Geophys. Res. 96, 13179–13188. https://doi.org/10.1029/91JD00054.

Gat, J.R., Bowser, C.J., Kendall, C., 1994. The contribution of evaporation from the Great Lakes to the continental atmosphere: estimate based on stable isotope data. Geophys. Res. Lett. 21, 557–560. https://doi.org/10.1029/94GL00069.

Gat, J.R., 1996. Oxygen and hydrogen isotopes in the hydrological cycle. Annu. Rev. Earth Planet. Sci. Lett. 24, 225–262. https://doi.org/10.1146/annurev.earth.24.1.225.

Gat, J.R., Airey, P.L., 2006. Stable water isotopes in the atmosphere/biosphere/lithosphere interface: scaling-up from the local to continental scale, under humid and dry conditions. Glob. Planet. Chang. 51, 25–33. https://doi.org/10.1016/j.gloplacha.2005.12.004.

Gázquez, F., Morellón, M., Bauska, T., Herwartz, D., Surma, J., Moreno, A., Staubwasser, M., Valero-Garcés, B., Delgado-Huertas, A., Hodell, D.A., 2018. Triple oxygen and hydrogen isotopes of gypsum hydration water for quantitative paleo-humidity reconstruction. Earth Planet. Sci. Lett. 481, 177–188. https://doi.org/10.1016/j.epsl.2017.10.020.

Giménez, R., Bartolomé, M., Gázquez, F., Iglesias, M., Moreno, A., 2021. Underlying climate controls in triple oxygen (^{16}O, ^{17}O, ^{18}O) and hydrogen (^{1}H, ^{2}H) isotopes composition of rainfall (central Pyrenees). Front. Earth Sci. 9 https://doi.org/10.3389/feart.2021.633698.

Gonfiantini, R., Wassenaar, L.I., Araguas-Araguas, L., Aggarwal, P.K., 2018. A unified Craig-Gordon isotope model of stable hydrogen and oxygen isotope fractionation during fresh or saltwater evaporation. Geochim. Cosmochim. Acta 235, 224–236. https://doi.org/10.1016/j.gca.2018.05.020.

Good, S.P., Noone, D., Bowen, G., 2015. Hydrologic connectivity constrains partitioning of global terrestrial water fluxes. Science 349, 175–177. https://doi.org/10.1126/science.aaa5931.

Graf, P., Wernli, H., Pfahl, S., Sodemann, H., 2019. A new interpretative framework for below-cloud effects on stable water isotopes in vapour and rain. Atmos. Chem. Phys. 19, 747–765. https://doi.org/10.5194/acp-19-747-2019.

Güntner, A., Stuck, J., Werth, S., Döll, P., Verzano, K., Merz, B., 2007. A global analysis of temporal and spatial variations in continental water storage. Water Resour. Res. 43, W05416. https://doi.org/10.1029/2006WR005247.

He, S., Jackisch, D., Samanta, D., Yi, P.K.Y., Liu, G., Wang, X., Goodkin, N.F., 2021. Understanding tropical convection through triple oxygen isotopes of precipitation from the Maritime Continent. J. Geophys. Res. Atmos. 126, e2020JD033418 https://doi.org/10.1029/2020JD033418.

Hellmann, R., Harvey, A.H., 2020. First-principles diffusivity ratios for kinetic isotope fractionation of water in air. Geophys. Res. Lett. 47, e2020GL089999 https://doi.org/10.1029/2020GL089999.

Hendricks, M.B., DePaolo, D.J., Cohen, R.C., 2000. Space and time variation of $\delta^{18}O$ and δD in precipitation: can paleotemperature be estimated from ice cores? Glob. Biogeochem. Cycles 14, 851–861. https://doi.org/10.1029/1999GB001198.

Hersbach, H., Bell, B., Berrisford, P., Hirahara, S., Horányi, A., Muñoz-Sabater, J., Nicolas, J., Peubey, C., Radu, R., Schepers, D., Simmons, A., Soci, C., Abdalla, S., Abellan, X., Balsamo, G., Bechtold, P., Biavati, G., Bidlot, J., Bonavita, M., De Chiara, G., Dahlgren, P., Dee, D., Diamantakis, M., Dragani, R., Flemming, J., Forbes, R., Fuentes, M., Geer, A., Haimberger, L., Healy, S., Hogan, R.J., Hólm, E., Janisková, M., Keeley, S., Laloyaux, P., Lopez, P., Lupu, C., Radnoti, G., de Rosnay, P., Rozum, I., Vamborg, F., Villaume, S., Thépaut, J.-N., 2020. The ERA5 global reanalysis. Q. J. R. Meteorol. Soc. 146, 1999–2049. https://doi.org/10.1002/qj.3803.

IAEA/WMO, 2022. The Global Network of Isotopes in Precipitation database. https://www.iaea.org/services/networks/gnip.

Johnsen, S.J., Dansgaard, W., White, J.W.C., 1989. The origin of Arctic precipitation under present and glacial conditions. Tellus B 41, 452–468. https://doi.org/10.3402/tellusb.v41i4.15100.

Jouzel, J., Merlivat, L., 1984. Deuterium and oxygen 18 in precipitation: modeling of the isotopic effects during snow formation. J. Geophys. Res. 89, 11749–11757. https://doi.org/10.1029/JD089iD07p11749.

Jouzel, J., Koster, R.D., 1996. A reconsideration of the initial conditions used for stable water isotope models. J. Geophys. Res. 101, 22933–22938. https://doi.org/10.1029/96JD02362.

Kelson, J.R., Petersen, S.V., Niemi, N.A., Passey, B.H., Curley, A.N., 2022. Looking upstream with clumped and triple oxygen isotopes of estuarine oyster shells in the early Eocene of California, USA. Geology. https://doi.org/10.1130/G49634.1.

Kong, Y., Pang, Z., Froehlich, K., 2013. Quantifying recycled moisture fraction in precipitation of an arid region using deuterium excess. Tellus B 65, 19251. https://doi.org/10.3402/tellusb.v65i0.19251.

Kopec, B.G., Feng, X., Posmentier, E.S., Sonder, L.J., 2019. Seasonal deuterium excess variations of precipitation at Summit, Greenland, and their climatological significance. J. Geophys. Res. Atmos. 124, 72–91. https://doi.org/10.1029/2018JD028750.

Kurita, N., 2013. Water isotopic variability in response to mesoscale convective system over the tropical ocean. J. Geophys. Res. Atmos. 118, 10376–10390. https://doi.org/10.1002/jgrd.50754.

Lamb, K.D., Clouser, B.W., Bolot, M., Sarkozy, L., Ebert, V., Saathoff, H., Möhler, O., Moyer, E.J., 2017. Laboratory measurements of HDO/H_2O isotopic fractionation during ice deposition in simulated cirrus clouds. Proc. Natl. Acad. Sci. 114, 5612–5617. https://doi.org/10.1073/pnas.1618374114.

Landais, A., Barkan, E., Luz, B., 2008. Record of $\delta^{18}O$ and ^{17}O-excess in ice from Vostok Antarctica during the last 150,000 years. Geophys. Res. Lett. 35, L02709. https://doi.org/10.1029/2007GL032096.

Landais, A., Risi, C., Bony, S., Vimeux, F., Descroix, L., Falourd, S., Bouygues, A., 2010. Combined measurements of $^{17}O_{excess}$ and d-excess in African monsoon precipitation: implications for evaluating convective parameterizations. Earth Planet. Sci. Lett. 298, 104–112. https://doi.org/10.1016/j.epsl.2010.07.033.

Landais, A., Ekaykin, A., Barkan, E., Winkler, R., Luz, B., 2012a. Seasonal variations of ^{17}O-excess and d-excess in snow precipitation at Vostok station, East Antarctica. J. Glaciol. 58, 725–733. https://doi.org/10.3189/2012JoG11J237.

Landais, A., Steen-Larsen, H.C., Guillevic, M., Masson-Delmotte, V., Vinther, B., Winkler, R., 2012b. Triple isotopic composition of oxygen in surface snow and water vapor at NEEM (Greenland). Geochim. Cosmochim. Acta 77, 304–316. https://doi.org/10.1016/j.gca.2011.11.022.

Landais, A., Capron, E., Masson-Delmotte, V., Toucanne, S., Rhodes, R., Popp, T., Vinther, B., Minster, B., Prié, F., 2018. Ice core evidence for decoupling between midlatitude atmospheric water cycle and Greenland temperature during the last deglaciation. Clim. Past 14, 1405–1415. https://doi.org/10.5194/cp-14-1405-2018.

Lee, J.-E., Fung, I., 2008. "Amount effect" of water isotopes and quantitative analysis of post-condensation processes. Hydrol. Process. 22, 1–8. https://doi.org/10.1002/hyp.6637.

Leuenberger, M.C., Ranjan, S., 2021. Disentangle kinetic from equilibrium fractionation using primary ($\delta^{17}O$, $\delta^{18}O$, δD) and secondary ($\Delta^{17}O$, d_{ex}) stable isotope parameters on samples from the Swiss Precipitation Network. Front. Earth Sci. 9 https://doi.org/10.3389/feart.2021.598061.

Li, L., Garzione, C.N., 2017. Spatial distribution and controlling factors of stable isotopes in meteoric waters on the Tibetan Plateau: implications for paleoelevation reconstruction. Earth Planet. Sci. Lett. 460, 302–314. https://doi.org/10.1016/j.epsl.2016.11.046.

Li, S., Levin, N.E., Chesson, L.A., 2015. Continental scale variation in ^{17}O-excess of meteoric waters in the United States. Geochim. Cosmochim. Acta 164, 110–126. https://doi.org/10.1016/j.gca.2015.04.047.

Liebminger, A., Haberhauer, G., Papesch, W., Heiss, G., 2006. Correlation of the isotopic composition in precipitation with local conditions in alpine regions. J. Geophys. Res. 111, D05104. https://doi.org/10.1029/2005JD006258.

Lohmann, U., Henneberger, J., Henneberg, O., Fugal, J.P., Bühl, J., Kanji, Z.A., 2016. Persistence of orographic mixed-phase clouds. Geophys. Res. Lett. 43, 10512–10519. https://doi.org/10.1002/2016GL071036.

Luz, B., Barkan, E., 2010. Variations of $^{17}O/^{16}O$ and $^{18}O/^{16}O$ in meteoric waters. Geochim. Cosmochim. Acta 74, 6276–6286. https://doi.org/10.1016/j.gca.2010.08.016.

Majoube, M., 1971a. Fractionnement en oxygène 18 et en deutérium entre l'eau et sa vapeur. J. Chim. Phys. 68, 1423–1436.

Majoube, M., 1971b. Fractionnement en ^{18}O entre la glace et la vapeur d'eau. J. Chim. Phys. 68, 625–636.

Markle, B.R., Steig, E.J., Buizert, C., Schoenemann, S.W., Bitz, C.M., Fudge, T.J., Pedro, J. B., Ding, Q., Jones, T.R., White, J.W.C., Sowers, T., 2017. Global atmospheric teleconnections during Dansgaard-Oeschger events. Nat. Geosci. 10, 36–40. https://doi.org/10.1038/ngeo2848.

Martens, B., Miralles, D.G., Lievens, H., van der Schalie, R., de Jeu, R.A.M., Fernández-Prieto, D., Beck, H.E., Dorigo, W.A., Verhoest, N.E.C., 2017. GLEAM v3: Satellite-based land evaporation and root-zone soil moisture. Geosci. Model Dev. 10, 1903–1925. https://doi.org/10.5194/gmd-10-1903-2017.

Maxwell, R.M., Condon, L.E., 2016. Connections between groundwater flow and transpiration partitioning. Science 353, 377–380. https://doi.org/10.1126/science.aaf7891.

Meijer, H.A.J., Li, W.J., 1998. The use of electrolysis for accurate $\delta^{17}O$ and $\delta^{18}O$ isotope measurements in water. Isot. Environ. Health Stud. 34, 349–369. https://doi.org/10.1080/10256019808234072.

Merlivat, L., Nief, G., 1967. Fractionnement isotopique lors des changements d'état solide-vapeur et liquide-vapeur de l'eau à des températures inférieures à 0°C. Tellus 19, 122–127. https://doi.org/10.1111/j.2153-3490.1967.tb01465.x.

Merlivat, L., 1978. Molecular diffusivities of $H_2^{16}O$, $HD^{16}O$, and $H_2^{18}O$ in gases. J. Chem. Phys. 69, 2864–2871. https://doi.org/10.1063/1.436884.

Merlivat, L., Jouzel, J., 1979. Global climatic interpretation of the deuterium-oxygen 18 relationship for precipitation. J. Geophys. Res. 84, 5029–5033. https://doi.org/10.1029/JC084iC08p05029.

Miller, M.F., 2002. Isotopic fractionation and the quantification of ^{17}O anomalies in the oxygen three-isotope system: an appraisal and geochemical significance. Geochim. Cosmochim. Acta 66, 1881–1889. https://doi.org/10.1016/S0016-7037(02)00832-3.

Miller, M.F., 2018. Precipitation regime influence on oxygen triple-isotope distributions in Antarctic precipitation and ice cores. Earth Planet. Sci. Lett. 481, 316–327. https://doi.org/10.1016/j.epsl.2017.10.035.

Pang, H., Hou, S., Landais, A., Masson-Delmotte, V., Prie, F., Steen-Larsen, H.C., Risi, C., Li, Y., Jouzel, J., Wang, Y., He, J., Minster, B., Falourd, S., 2015. Spatial distribution of ^{17}O-excess in surface snow along a traverse from Zhongshan station to Dome A, East Antarctica. Earth Planet. Sci. Lett. 414, 126–133. https://doi.org/10.1016/j.epsl.2015.01.014.

Pang, H., Hou, S., Landais, A., Masson-Delmotte, V., Jouzel, J., Steen-Larsen, H.C., Risi, C., Zhang, W., Wu, S., Li, Y., An, C., Wang, Y., Prie, F., Minster, B., Falourd, S., Stenni, B., Scarchilli, C., Fujita, K., Grigioni, P., 2019. Influence of summer sublimation on δD, $\delta^{18}O$, and $\delta^{17}O$ in precipitation, East Antarctica, and implications for climate reconstruction from ice cores. J. Geophys. Res. Atmos. 124, 7339–7358. https://doi.org/10.1029/2018JD030218.

Pang, Z., Kong, Y., Froehlich, K., Huang, T., Yuan, L., Li, Z., Wang, F., 2011. Processes affecting isotopes in precipitation of an arid region. Tellus B 63, 352–359. https://doi.org/10.1111/j.1600-0889.2011.00532.x.

Passey, B.H., Hu, H., Ji, H., Montanari, S., Li, S., Henkes, G.A., Levin, N.E., 2014. Triple oxygen isotopes in biogenic and sedimentary carbonates. Geochim. Cosmochim. Acta 141, 1–25. https://doi.org/10.1016/j.gca.2014.06.006.

Passey, B.H., Levin, N.E., 2021. Triple oxygen isotopes in meteoric waters, carbonates, and biological apatites: Implications for continental paleoclimate reconstruction. Rev. Mineral. Geochem. 86, 429–462. https://doi.org/10.2138/rmg.2021.86.13.

Petit, J.R., White, J.W.C., Young, N.W., Jouzel, J., Korotkevich, Y.S., 1991. Deuterium excess in recent Antarctic snow. J. Geophys. Res. 96, 5113–5122. https://doi.org/10.1029/90JD02232.

Pfahl, S., Wernli, H., 2009. Lagrangian simulations of stable isotopes in water vapor: an evaluation of nonequilibrium fractionation in the Craig-Gordon model. J. Geophys. Res. 114, D20108. https://doi.org/10.1029/2009JD012054.

Pfahl, S., Sodemann, H., 2014. What controls deuterium excess in global precipitation? Clim.Past. 10, 771–781. https://doi.org/10.5194/cp-10-771-2014.

Pierchala, A., Rozanski, K., Dulinski, M., Gorczyca, Z., 2022. Quantification the diffusion-induced fractionation of $^{1}H_{2}^{17}O$ isotopologue in air accompanying the process of water evaporation. Geochim. Cosmochim. Acta 322, 244–259. https://doi.org/10.1016/j.gca.2022.01.020.

Putman, A.L., Fiorella, R.P., Bowen, G.J., Cai, Z., 2019. A global perspective on local meteoric water lines: meta-analytic insight into fundamental controls and practical constraints. Water Resour. Res. 55, 6896–6910. https://doi.org/10.1029/2019WR025181.

Risi, C., Bony, S., Vimeux, F., 2008. Influence of convective processes on the isotopic composition ($\delta^{18}O$ and δD) of precipitation and water vapor in the tropics: 2. Physical interpretation of the amount effect. J. Geophys. Res. Atmos. 113, D19306 https://doi.org/10.1029/2008JD009943.

Risi, C., Bony, S., Vimeux, F., Jouzel, J., 2010a. Water-stable isotopes in the LMDZ4 general circulation model: model evaluation for present-day and past climates and applications to climatic interpretations of tropical isotopic records. J. Geophys. Res. 115, D12118. https://doi.org/10.1029/2009JD013255.

Risi, C., Landais, A., Bony, S., Jouzel, J., Masson-Delmotte, V., Vimeux, F., 2010b. Understanding the ^{17}O excess glacial-interglacial variations in Vostok precipitation. J. Geophys. Res. 115, D10112. https://doi.org/10.1029/2008JD011535.

Risi, C., Noone, D., Worden, J., Frankenberg, C., Stiller, G., Kiefer, M., Funke, B., Walker, K., Bernath, P., Schneider, M., Wunch, D., Sherlock, V., Deutscher, N., Griffith, D., Wennberg, P.O., Strong, K., Smale, D., Mahieu, E., Barthlott, S., Hase, F., García, O., Notholt, J., Warneke, T., Toon, G., Sayres, D., Bony, S., Lee, J., Brown, D., Uemura, R., Sturm, C., 2012. Process-evaluation of tropospheric humidity simulated by general circulation models using water vapor isotopologues: 1. Comparison between models and observations. J. Geophys. Res. 117, D05303 https://doi.org/10.1029/2011JD016621.

Risi, C., Landais, A., Winkler, R., Vimeux, F., 2013. Can we determine what controls the spatio-temporal distribution of d-excess and ^{17}O-excess in precipitation using the LMDZ general circulation model? Clim.Past. 9, 2173–2193. https://doi.org/10.5194/cp-9-2173-2013.

Schauer, A.J., Schoenemann, S.W., Steig, E.J., 2016. Routine high-precision analysis of triple water-isotope ratios using cavity ring-down spectroscopy. Rapid Commun. Mass Spectrom. 30, 2059–2069. https://doi.org/10.1002/rcm.7682.

Schoenemann, S.W., Schauer, A.J., Steig, E.J., 2013. Measurement of SLAP2 and GISP $\delta^{17}O$ and proposed VSMOW-SLAP normalization for $\delta^{17}O$ and $^{17}O_{excess}$. Rapid Commun. Mass Spectrom. 27, 582–590. https://doi.org/10.1002/rcm.6486.

Schoenemann, S.W., Steig, E.J., Ding, Q., Markle, B.R., Schauer, A.J., 2014. Triple water-isotopologue record from WAIS divide, Antarctica: controls on glacial-interglacial changes in $^{17}O_{excess}$ of precipitation. J. Geophys. Res. Atmos. 119, 8741–8763. https://doi.org/10.1002/2014JD021770.

Schoenemann, S.W., Steig, E.J., 2016. Seasonal and spatial variations of $^{17}O_{excess}$ and dexcess in Antarctic precipitation: insights from an intermediate complexity isotope model. J. Geophys. Res. Atmos. 121, 11215–11247. https://doi.org/10.1002/2016JD025117.

Sha, L., Mahata, S., Duan, P., Luz, B., Zhang, P., Baker, J., Zong, B., Ning, Y., Brahim, Y. A., Zhang, H., Edwards, R.L., Cheng, H., 2020. A novel application of triple oxygen isotope ratios of speleothems. Geochim. Cosmochim. Acta 270, 360–378. https://doi.org/10.1016/j.gca.2019.12.003.

Shao, L., Tian, L., Cai, Z., Wang, C., Li, Y., 2021. Large-scale atmospheric circulation influences the ice core d-excess record from the central Tibetan Plateau. Clim. Dyn. 57, 1805–1816. https://doi.org/10.1007/s00382-021-05779-9.

Sharp, Z.D., Wostbrock, J.A.G., Pack, A., 2018. Mass-dependent triple oxygen isotope variations in terrestrial materials. Geochem. Perspect. Lett. 7, 27–31. https://doi.org/10.7185/geochemlet.1815.

Steen-Larsen, H.C., Sveinbjörnsdottir, A.E., Peters, A.J., Masson-Delmotte, V., Guishard, M.P., Hsiao, G., Jouzel, J., Noone, D., Warren, J.K., White, J.W.C., 2014. Climatic controls on water vapor deuterium excess in the marine boundary layer of the North Atlantic based on 500 days of in situ, continuous measurements. Atmos. Chem. Phys. 14, 7741–7756. https://doi.org/10.5194/acp-14-7741-2014.

Steig, E.J., Jones, T.R., Schauer, A.J., Kahle, E.C., Morris, V.A., Vaughn, B.H., Davidge, L., White, J.W.C., 2021. Continuous-flow analysis of $\delta^{17}O$, $\delta^{18}O$, and δD of H_2O on an ice core from the South Pole. Front. Earth Sci. 9 https://doi.org/10.3389/feart.2021.640292.

Stenni, B., Masson-Delmotte, V., Johnsen, S., Jouzel, J., Longinelli, A., Monnin, E., Röthlisberger, R., Selmo, E., 2001. An oceanic cold reversal during the last deglaciation. Science 293, 2074–2077. https://doi.org/10.1126/science.1059702.

Stewart, M.K., 1975. Stable isotope fractionation due to evaporation and isotopic exchange of falling waterdrops: applications to atmospheric processes and evaporation of lakes. J. Geophys. Res. 80, 1133–1146. https://doi.org/10.1029/JC080i009p01133.

Surma, J., Assonov, S., Bolourchi, M.J., Staubwasser, M., 2015. Triple oxygen isotope signatures in evaporated water bodies from the Sistan Oasis, Iran. Geophys. Res. Lett. 42, 8456–8462. https://doi.org/10.1002/2015GL066475.

Surma, J., Assonov, S., Herwartz, D., Voigt, C., Staubwasser, M., 2018. The evolution of ^{17}O-excess in surface water of the arid environment during recharge and evaporation. Sci. Rep. 8, 4972. https://doi.org/10.1038/s41598-018-23151-6.

Surma, J., Assonov, S., Staubwasser, M., 2021. Triple oxygen isotope systematics in the hydrologic cycle. Rev. Mineral. Geochem. 86, 401–428. https://doi.org/10.2138/rmg.2021.86.12.

Tian, C., Wang, L., Kaseke, K.F., Bird, B.W., 2018. Stable isotope compositions ($\delta^{2}H$, $\delta^{18}O$ and $\delta^{17}O$) of rainfall and snowfall in the Central United States. Sci. Rep. 8, 6712. https://doi.org/10.1038/s41598-018-25102-7.

Tian, C., Wang, L., Tian, F., Zhao, S., Jiao, W., 2019. Spatial and temporal variations of tap water ^{17}O-excess in China. Geochim. Cosmochim. Acta 260, 1–14. https://doi.org/10.1016/j.gca.2019.06.015.

Uechi, Y., Uemura, R., 2019. Dominant influence of the humidity in the moisture source region on the ^{17}O-excess in precipitation on a subtropical island. Earth Planet. Sci. Lett. 513, 20–28. https://doi.org/10.1016/j.epsl.2019.02.012.

Uemura, R., Matsui, Y., Yoshimura, K., Motoyama, H., Yoshida, N., 2008. Evidence of deuterium excess in water vapor as an indicator of ocean surface conditions. J. Geophys. Res. 113, D19114. https://doi.org/10.1029/2008JD010209.

Uemura, R., Barkan, E., Abe, O., Luz, B., 2010. Triple isotope composition of oxygen in atmospheric water vapor. Geophys. Res. Lett. 37, L04402. https://doi.org/10.1029/2009GL041960.

Uemura, R., Masson-Delmotte, V., Jouzel, J., Landais, A., Motoyama, H., Stenni, B., 2012. Ranges of moisture-source temperature estimated from Antarctic ice cores stable isotope records over glacial–interglacial cycles. Clim. Past 8, 1109–1125. https://doi.org/10.5194/cp-8-1109-2012.

van Breukelen, M.R., Vonhof, H.B., Hellstrom, J.C., Wester, W.C.G., Kroon, D., 2008. Fossil dripwater in stalagmites reveals Holocene temperature and rainfall variation in Amazonia. Earth Planet. Sci. Lett. 275, 54–60. https://doi.org/10.1016/j.epsl.2008.07.060.

Van Hook, W.A., 1968. Vapor pressures of the isotopic waters and ices. J. Phys. Chem. 72, 1234–1244. https://doi.org/10.1021/j100850a028.

Vimeux, F., Masson, V., Jouzel, J., Stievenard, M., Petit, J.R., 1999. Glacial–interglacial changes in ocean surface conditions in the Southern Hemisphere. Nature 398, 410–413. https://doi.org/10.1038/18860.

Voigt, C., Herwartz, D., Dorador, C., Staubwasser, M., 2021. Triple oxygen isotope systematics of evaporation and mixing processes in a dynamic desert lake system. Hydrol. Earth Syst. Sci. 25, 1211–1228. https://doi.org/10.5194/hess-25-1211-2021.

Wang, S., Zhang, M., Che, Y., Chen, F., Qiang, F., 2016a. Contribution of recycled moisture to precipitation in oases of arid Central Asia: a stable isotope approach. Water Resour. Res. 52, 3246–3257. https://doi.org/10.1002/2015WR018135.

Wang, S., Zhang, M., Che, Y., Zhu, X., Liu, X., 2016b. Influence of below-cloud evaporation on deuterium excess in precipitation of arid Central Asia and its meteorological controls. J. Hydrometeorol. 17, 1973–1984. https://doi.org/10.1175/JHM-D-15-0203.1.

Wassenaar, L., Terzer-Wassmuth, S., Douence, C., 2021. Progress and challenges in dual- and triple-isotope ($\delta^{18}O$, $\delta^{2}H$, $\Delta^{17}O$) analyses of environmental waters: an international assessment of laboratory performance. Rapid Commun. Mass Spectrom. 35, e9193 https://doi.org/10.1002/rcm.9193.

Wei, Z., Lee, X., 2019. The utility of near-surface water vapor deuterium excess as an indicator of atmospheric moisture source. J. Hydrol. 577, 123923 https://doi.org/10.1016/j.jhydrol.2019.123923.

Werner, M., Langebroek, P.M., Carlsen, T., Herold, M., Lohmann, G., 2011. Stable water isotopes in the ECHAM5 general circulation model: toward high-resolution isotope modeling on a global scale. J. Geophys. Res. Atmos. 116, D15109. https://doi.org/10.1029/2011JD015681.

Winkler, R., Landais, A., Sodemann, H., Dümbgen, L., Prié, F., Masson-Delmotte, V., Stenni, B., Jouzel, J., 2012. Deglaciation records of ^{17}O-excess in East Antarctica: reliable reconstruction of oceanic normalized relative humidity from coastal sites. Clim. Past 8, 1–16. https://doi.org/10.5194/cp-8-1-2012.

Winnick, M.J., Chamberlain, C.P., Caves, J.K., Welker, J.M., 2014. Quantifying the isotopic 'continental effect'. Earth Planet. Sci. Lett. 406, 123–133. https://doi.org/10.1016/j.epsl.2014.09.005.

Xia, Z., Winnick, M.J., 2021. The competing effects of terrestrial evapotranspiration and raindrop re-evaporation on the deuterium excess of continental precipitation. Earth Planet. Sci. Lett. 572, 117120 https://doi.org/10.1016/j.epsl.2021.117120.

Xia, Z., Welker, J.M., Winnick, M.J., 2022. The seasonality of deuterium excess in non-polar precipitation. Glob. Biogeochem. Cycles. 36, e2021GB007245 https://doi.org/10.1029/2021GB007245.

Xia, Z., 2023. Quantifying the fingerprint of oceanic moisture source conditions in deuterium and ^{17}O excess parameters of precipitation. Geophys. Res. Lett. 50, e2022GL101901 https://doi.org/10.1029/2022GL101901.